

VISCOSITY MEASUREMENT THROUGH STRETCHING OF LIQUID BRIDGE

A report

Submitted in partial fulfilment of the requirement for the degree of

Master of Technology
In the faculty of engineering

BY
PRAVIN AGARWAL

Under the guidance of
Prof. M. S. BOBBI



Department of Mechanical Engineering

Indian Institute of Science

Bangalore 560012, INDIA

June 2019

ACKNOWLEDGEMENTS

I would like to express my deep sense of gratitude and profound feelings of admiration to my guide Professor M. S. Bobji who gave me the opportunity to work with him. I am indebted to him for his interest in my work, for constant encouragement, critical suggestions and stimulating discussions. I am thankful to him for believing me and allowing me to work independently.

I express my gratitude toward the chairman of the mechanical department for giving me the opportunity for studying in the department. I especially thank Prof. KRY Simha for all his motivational encouragement and life lessons during my stay in IISc. I also give my deep respect to all professors who gave me inside depth knowledge of the theoretical world as well as the real world during my 'course work'. I am also thankful to the mechanical department for providing me with wonderful infrastructure.

My force microscopy laboratory (FM Lab) is a multi-disciplinary lab which provides a resourceful friendly environment for exploration of science. I sincerely thank all my labmates Dr Sudipta Dutta, Dr Muthu Kumar M, Mahesh Kumar Singh, Jeet Kumar Gaur, Gautam Revankar A, Raghavendra M and Aiswarya M for fruitful scientific discussions and their help. At last not least, I would like to acknowledge Mrs Sulochana EK and Mr Srinivasa Raghavan for their administrative and logistic support.

I would like to sincerely acknowledge and thank my parent organization, 'Defence Bioengineering and Electromedical Laboratory' (DEBEL), Bangalore, DRDO for sponsoring me for this post-graduation course. I am thankful to my friends for their timely support during this work. I am also grateful to my parents, wife Arati and both sons Arnav and Aaryav for their selfless love, support and constant faith in me. I also give my regards to others who helped me directly and indirectly.

Pravin Agarwal

ABSTRACT

Viscosity, which is an internal friction force, depends on cohesive forces and molecular momentum exchange, but other factors also may affect it i.e., diffusion. Generally, viscosity measurement is done on the bulk quantity where volumetric forces are more dominant compared to surface forces. When a small amount of fluid is subjected in relative motion, the magnitude of viscosity might significantly change from its bulk measurement; due to more relevance of surface forces. Measurement of viscosity of a small amount of liquid can reveal this phenomenon.

Formation of Liquid Bridge (LB) between two surfaces that are in close proximity has been of attention for decades. LB creates adhesive/repulsive forces between surfaces as per the shape of LB. In the static condition, only capillary force is considered in LB analysis. But, during stretching of LB, the added viscous force can't be neglected. Viscosity and LB have been discussed in large, but the study of viscosity with the help of the LB has not received attention.

An experimental setup is designed, and the results of the experiment are analysed in this work. Throughout the experiment, a tiny liquid drop, formed by silicone oil, DI Water or 1-Dodecanethiol, approximately one mm radius, is suspended between two moving surfaces for forming an LB. For stretching this LB, the displacement of one end of the LB is controlled by a linear actuator with the help of a stepper motor. The repulsive or attractive force from LB is measured by the deflection of the cantilever. Displacement of this tip is measured precisely by a fiber optic displacement sensor for calculating reaction force. Dimensions of an LB are measured with the help of a high-speed digital camera. A computer interface is developed for controlling the actuator and measuring the displacement of the cantilever tip, simultaneously using a high-speed data acquisition system.

Force vs displacement and force vs time, graphs for all three liquids are obtained and compared for repeatability and behaviour analysis. Due to negligible evaporation losses, 1-Dodecanethiol shows repeatability for experiments with wide stretch rates. Extensional viscosity is calculated by measuring the radius of cylindrical filament and breakup time, Magnitude of measured viscosity matches with the specified values in literature.

TABLE OF CONTENTS

ACKNOWLEDGEMENTS	ii
ABSTRACT.....	iii
LIST OF FIGURES	vii
1. INTRODUCTION	1
1.1. MOTIVATION	1
1.2. LIQUID BRIDGE FORMATION	2
1.3. NECESSITY OF THIS WORK.....	4
1.4. OBJECTIVES OF THIS WORK.....	4
2. LITERATURE REVIEW	6
2.1. INITIAL STUDIES ON LIQUID BRIDGE.....	6
2.2. STUDY OF STATIC FORCES IN LIQUID BRIDGE	6
2.3. DYNAMIC FORCES IN LIQUID BRIDGE	7
2.4. MEASUREMENT TECHNIQUES	8
2.5. THEORETICAL ANALYSIS IN LIQUID BRIDGE	8
2.5.1. ASSUMPTIONS	9
2.5.2. CAPILLARY FORCES IN LIQUID BRIDGE	11
2.5.3. CAPILLARY FORCE BY CONSTANT VOLUME APPROACH	15
2.5.4. VISCOUS FORCE IN LIQUID BRIDGE.....	15
2.6. MEASUREMENT METHODOLOGY FOR VISCOSITY	16
2.6.1. TROUTON RATIO.....	17
2.6.2. FIRST METHODOLOGY FOR VISCOSITY MEASUREMENT.....	17
2.6.3. SECOND METHODOLOGY FOR VISCOSITY MEASUREMENT.....	18

2.7.	MEASUREMENT OF CANTILEVER STIFFNESS BY ADDED MASS	19
3.	DEVELOPMENT OF EXPERIMENTAL SETUP	21
3.1.	FORCE MEASURING SUBSYSTEM FOR LIQUID BRIDGE.....	21
3.1.1.	DESIGN OF FORCE SENSOR.....	21
3.1.2.	DISPLACEMENT MEASUREMENT SUBSYSTEM	25
3.2.	IMAGE ACQUISITION SYSTEM.....	29
3.2.1.	SETUP OF TRINOCULAR WITH INTEGRATION OF USB CAMERA	29
3.3.	SUBSYSTEM FOR LINEAR STRETCHING OF LIQUID BRIDGE.....	30
3.3.1.	LINEAR ACTUATION FOR QUASI-STATIC STRETCHING.....	30
3.3.2.	LINEAR ACTUATION FOR CONTINUOUS STRETCHING	33
3.4.	LIQUID SAMPLES.....	36
3.4.1.	SILICONE ELASTOMER.....	36
3.4.2.	DI WATER	37
3.4.3.	1-DODECANETHIOL.....	37
4.	RESULTS	38
4.1.	QUASI-STATIC STRETCHING OF LIQUID BRIDGE	38
4.1.1.	DETAILS OF EXPERIMENT FOR QUASI-STATIC STRETCHING.....	38
4.1.2.	FORCE DISPLACEMENT CURVE FOR QUASI-STATIC STRETCHING... 38	
4.2.	EXPERIMENTS WITH CONTINUOUS STRETCHING OF LIQUID BRIDGE.. 40	
4.2.1.	EXPERIMENTAL SETUP FOR CONTINUOUS STRETCHING	40
4.2.2.	EXPERIMENT PROCEDURE FOR CONTINUOUS STRETCHING	41
4.3.	VISCOSITY MEASUREMENT	59
4.4.	DISCUSSION ON STRETCHING OF LIQUID BRIDGE EXPERIMENTS	62
5.	CONCLUSION AND FUTURE WORK	63

5.1. CONCLUSION.....	63
5.2. FUTURE SCOPE.....	64
REFERENCE.....	65

LIST OF FIGURES

Figure 1: Liquid bridge configuration between the sphere and flat surface	2
Figure 2: Stable static states of the liquid bridge[1]	3
Figure 3: Schematic of experimental setup for liquid bridge	5
Figure 4: Liquid Bridge between axisymmetric spherical particle and a planar solid surface	9
Figure 5: Liquid Bridge configuration	12
Figure 6: Sketch of a two-phase system composed of phases 1 and 2	13
Figure 7: Capillary force with constant volume approach [22]	15
Figure 8: Drawing & Prototypes of Cantilever.....	24
Figure 9: Plot between added mass (M) and $1/(2\pi\nu)^2$ for cantilever calibration	25
Figure 10: Experimental setup for calibration of Fiberoptic sensor	27
Figure 11: Characteristic of the fiber optic sensor.....	28
Figure 12: Near side Characteristic of fiberoptic sensor	28
Figure 13: Far side Characteristic of fiberoptic sensor	29
Figure 14: USB Camera (mvBlueFOX-IGC) [27].....	30
Figure 15: Assembly of Trinocular with USB Camera and digital camera	30
Figure 16: Experimental setup for characterization of Piezo XYZ stage (Nano cube)	32
Figure 17: Micro stage, Model M3-LS-1.8-6, Make NewScale	32
Figure 18: Linear actuator with stepper motor	34
Figure 19: Microstep driver for stepper motor	34
Figure 20: Expected displacement of stepper motor.....	35
Figure 21: Measured displacement of Stepper motor in Volts before applying damper	35
Figure 22: Isolation of vibration from the linear actuator.....	35
Figure 23: Measured displacement of Stepper motor in Volts after applying damper	36

Figure 24: Experiment setup for quasi-static stretching	39
Figure 25: Liquid bridge formation during quasi-static stretching	39
Figure 26: Micro Stage displacement vs Cantilever reaction force for silicone oil drop.	40
Figure 27: Experimental setup with continuous motion	41
Figure 28: Force vs displacement curve with Raw data for silicone elastomer with a stretch rate of 133 $\mu\text{m/s}$	43
Figure 29: Raw data is filtered with 100 points moving average (snapshot of data at the jump in contact) for silicone.....	44
Figure 30: Filtered force vs displacement curve for silicone with a stretch rate of 133 $\mu\text{m/s}$	44
Figure 31: Filtered force vs displacement curve for silicone with a stretch rate of 190 $\mu\text{m/s}$	45
Figure 32: Filtered force vs displacement curve for silicone with a stretch rate of 228 $\mu\text{m/s}$	45
Figure 33: Compare force vs displacement curve for silicone with the different stretch rates	46
Figure 34: Filtered force vs time curve for silicone elastomer with a stretch rate of 228 $\mu\text{m/s}$...	46
Figure 35: Pictures of the liquid bridge formed by silicone with marked regimes.....	47
Figure 36: Force vs displacement curve with Raw data for DI water with a stretch rate of 190 $\mu\text{m/s}$	49
Figure 37: Raw data is filtered with 100 points moving average (snapshot of data at breakup) for DI water	49
Figure 38: Filtered force vs displacement curve for DI water with a stretch rate of 190 $\mu\text{m/s}$	50
Figure 39: Filtered force vs displacement curve for DI water with a stretch rate of 38 $\mu\text{m/s}$	50
Figure 40: Compare with Filtered force vs displacement curve for DI water with different stretch rates	51
Figure 41: Filtered force vs time curve for DI water with a stretch rate of 190 $\mu\text{m/s}$	51
Figure 42: Pictures of the liquid bridge formed by DI water with marked regimes.....	52

Figure 43: Force vs displacement curve with Raw data for 1-Dodecanethiol with the stretch rate of 38 $\mu\text{m/s}$	54
Figure 44: Raw data is filtered with 100 points moving average (snapshot of data at breakup) for 1-dodecanethiol.....	54
Figure 45: Filtered force vs displacement curve for 1-dodecanethiol with stretch rate 38 $\mu\text{m/s}$.	55
Figure 46: Filtered force vs displacement curve for 1-dodecanethiol with stretch rate 114 $\mu\text{m/s}$	55
Figure 47: Filtered force vs displacement curve for 1-dodecanethiol with stretch rate 228 $\mu\text{m/s}$	56
Figure 48: Compare with force vs displacement curve for 1-Dodecanethiol with different stretch rate.....	56
Figure 49: Filtered force vs time curve for 1-Dodecanethiol with stretch rate 114 $\mu\text{m/s}$	57
Figure 50: Filtered force vs time curve for 1-Dodecanethiol with stretch rate 228 $\mu\text{m/s}$	57
Figure 51: Pictures of the liquid bridge formed by 1-Dodecanethiol with marked regimes	58
Figure 52: Liquid bridge after stretching and holding	60
Figure 53: Neck of the liquid bridge, transforms in a cylindrical shape.....	60
Figure 54: Intermediate frames of automatic depletion of the liquid bridge	61

CHAPTER-1

1. INTRODUCTION

Body forces e.g., gravity depends on the volume of matter but surface forces e.g., surface tension depends on the area of matter. While the size of the matter reduces, reduction of body forces happens in one order magnitude more as compared to surface forces. So, the relevance of surface forces become more as compared to volume force at the micro level.

1.1. MOTIVATION

Viscosity tries to hinder the motion of a physical device or an object. Generally, it is understood that viscosity is an intensive property of any fluid i.e., it does not depend on the size of fluid. But it may depend on the size of the subjected fluid also. The viscosity of fluid shall be known before estimation of power required for different applications e.g., atomization (liquid droplets), mixing, the design of pipelines, pump characteristics, storage, injection, and transportation.

Viscosity is referred to as friction between the molecules of a fluid which opposes the relative motion between two surfaces of the fluid that are moving at different velocities. The viscosity of a fluid, term as drag force, is the measure of its resistance to gradual deformation when external shear stress or tensile stress is applied on fluid. Viscosity is an effect of cohesive force and molecular momentum exchange in the fluid. The viscosity of fluid depends on the magnitude of strain rate, temperature, and pressure, etc. It is well known, when the temperature rises, the viscosity of liquids decreases but the viscosity of gases increases. Viscosity is expressed as different ways e.g., dynamic viscosity, kinematic viscosity, shear viscosity, dilatational viscosity and extension viscosity, etc. Viscosity is generally measured with an only bulk quantity of fluid but there is lack of information about the viscosity of micro scale of the fluid.

Qualitative analysis of viscosity of the tiny liquid is regularly is done in our kitchens. The readiness of sugar syrup, used for desserts, is checked by forming a filament between thumb and finger. The number of filaments is an indication of the measurement of viscosity of the sugar syrup.

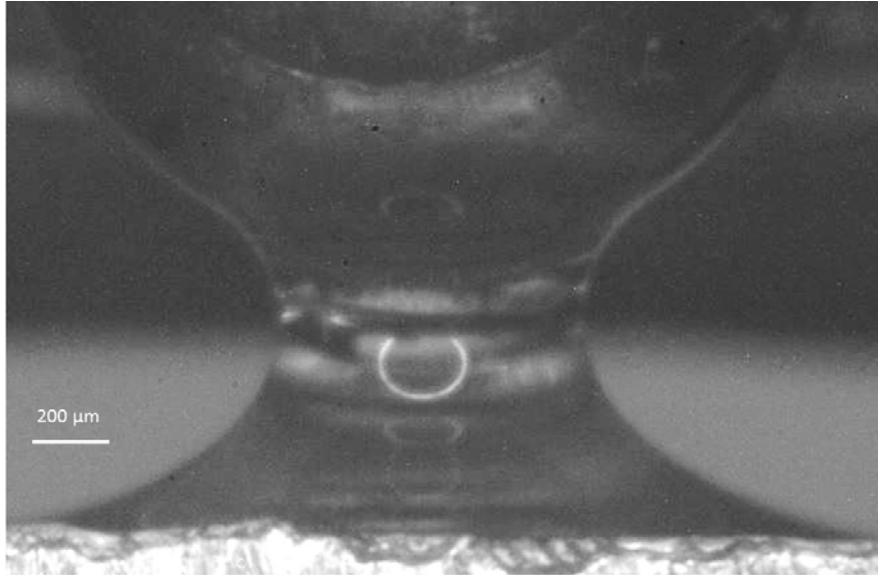


Figure 1: Liquid bridge configuration between the sphere and flat surface

1.2. LIQUID BRIDGE FORMATION

When a small amount of liquid is held in contact between two near contacting surfaces than the liquid bridge, as shown in Figure 1, is formed. The liquid bridge is also referred to as menisci, water-bridge or capillary bridge in literature. Formation of this liquid bridge is the result of the minimization of surface energy. Generally, the profile of the liquid bridge is formed as convex, cylindrical or concave which depends on the nature of the surface[1]. These profiles of the liquid bridge, as shown in Figure 2, are the result of surface tension between interacting surfaces. Two hydrophilic surfaces forms concave-shaped, two hydrophobic surfaces forms convex-shape and two neutral surfaces forms cylindrical-shape liquid bridge. For maintaining equilibrium position, negative pressure or attractive force is build up inside concave-shape and cylindrical-shape liquid bridges; positive pressure or repulsive force is built up inside the convex-shape liquid bridge. This resultant negative force creates high static friction which is called stiction in smooth surfaces during relative motion. The magnitude of this force depends on the area of the liquid bridge, contact angle and number of formed liquid bridges.

Liquid bridge configuration is found in many places such as cohesion of moist soils, powder granulation, printing, ‘flow in porous media’, liquid-phase sintering, soldering process, etc. The escalation in the strength of powders due to the absorption of humidity from the surroundings,

leading to flow and process-related problems, has been studied since the late 1960s. Small liquid as moisture in sand or soil gives strength to it. Forming a sandcastle is an example of this effect. But, excess liquid in soil destroys the binding force. A catastrophic example is landslides in hilly areas during rainy seasons. Liquid bridge formation is also used for the experimental study to determine the extensional viscosity of non-Newtonian fluids[2]. Results of atomic force microscope (AFM) can be affected by the appearance of Nano-sized capillary bridges in higher humidity environment[3],[4]. Tiny capillary bridges also affect many medical problems involving respiratory diseases and body joints[5]. Frogs, insects, lizards, and spiders also create adhesive force by forming a liquid bridge[6].

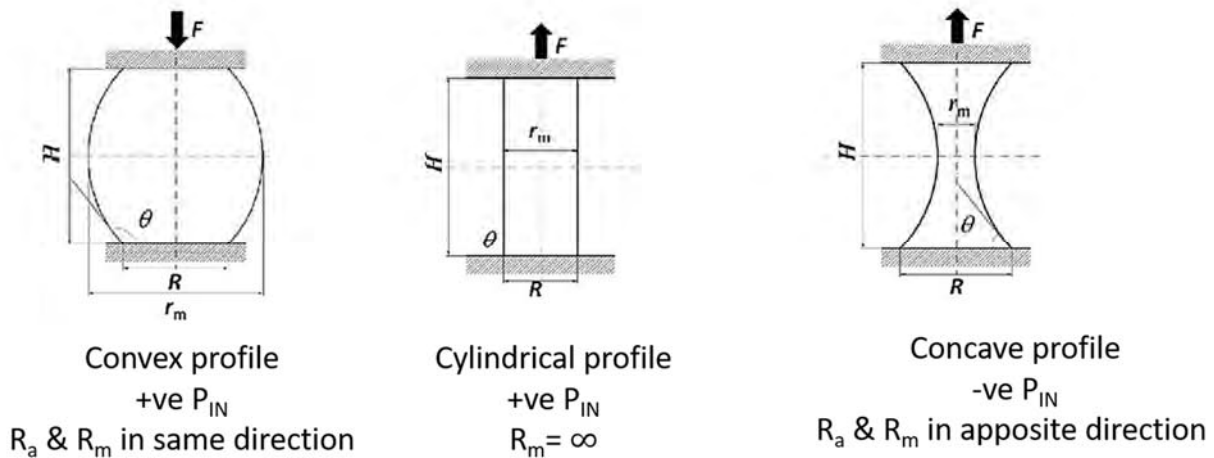


Figure 2: Stable static states of the liquid bridge[1]

(R_m : Meridional radii, R_a : Azimuthal radii & P_{in} : Inside Pressure)

Adhesion force due to the liquid bridge is a combination of surface tension, Laplace pressure, and viscosity. Force due to surface tension act on the periphery of the intersection of the liquid bridge and solid surface which holds the liquid bridge. Pressure buildup inside of liquid bridge is calculated by the Yong-Laplace equation in the static equilibrium condition. This Laplace pressure act on the cross-section area of the liquid bridge in the normal direction of the cross-section area. These two forces, due to surface tension and Laplace pressure in the liquid bridge, are jointly called capillary force or meniscus force. The capillary force acts only when the liquid bridge is in a static equilibrium condition. The adhesive force due to viscosity is added with capillary force in the liquid bridge during dynamic loading where stretching of liquid bridge happens in finite time.

1.3. NECESSITY OF THIS WORK

Analytical, as well as numerical solutions for an axisymmetric profile of liquid bridge in a static condition, are given by many pioneers in this field. Practical engineering design of micro-objects which involves liquid bridge formation can't be adequate by using only static analysis. During elongation of a liquid bridge, either capillary force or viscous force can be dominant. When elongation of the liquid bridge started by the dynamic load, capillary forces dominate on viscosity. But, near to breakup condition, viscosity effect dominates on the capillary force[7]. Study of the liquid bridge during elongation condition is given less attraction to researchers where viscosity plays a major role. Few researchers have given simulation results for dynamic loading condition also, but this research is not supported by experimental results[7]. Some researchers developed the methods of measurement of viscosity by measuring only the diameter of the liquid bridge before the breakup and the time required for breaking the liquid bridge. They did not measure reaction forces at the ends of the liquid bridge[8] for calculating viscosity.

Viscosity measured by the liquid bridge is an extensional viscosity because the force applied in the same direction of elongation of the liquid bridge, but shearing action happens at co-centric cylindrical surfaces inside the liquid bridge. Trouton ratio is defined as the ratio of extensional viscosity and shear viscosity. When one-dimensional elongation happens with very slow strain rate, Trouton ratio becomes three. Trouton ratio becomes very high for high strain rates. So, viscosity measured by the stretching of the liquid bridge will not be a constant number; it will depend on the applied strain rate.

Almost nil experimental results are discussed in the literature about the measurement of viscosity through stretching of liquid bridge. The measurement of viscosity by stretching of the liquid bridge is necessary for well understudying the physics behind the phenomena.

1.4. OBJECTIVES OF THIS WORK

The objective of this work is “measurement of extensional viscosity by stretching a liquid bridge formed between two rigid surfaces”. To achieve the required objective, an experimental setup for forming and controlled stretching of the liquid bridge is built up. This setup has the capability to

measure the reaction force in μN resolution at one end of the liquid bridge. The experimental setup is constructed for forming and stretching a liquid bridge as schematically shown in Figure 3.

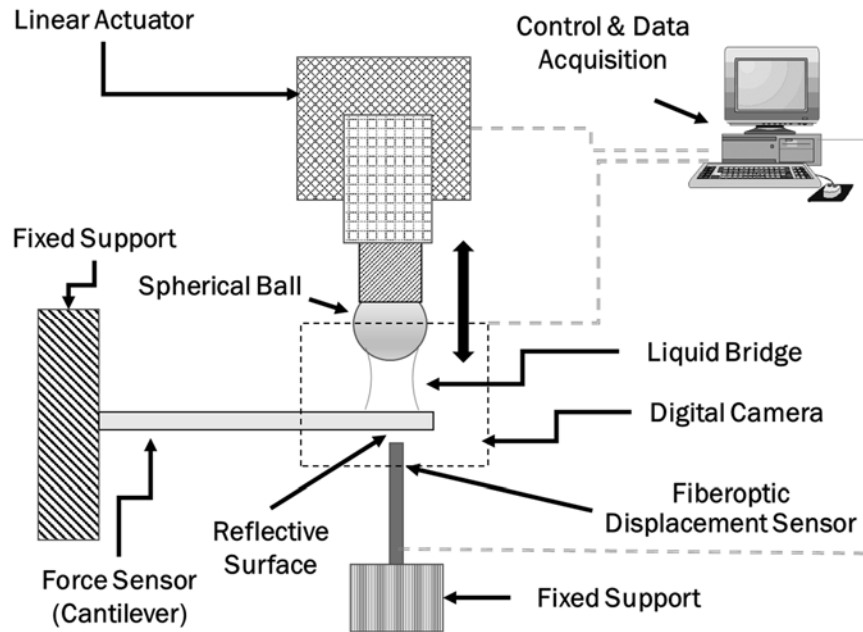


Figure 3: Schematic of experimental setup for liquid bridge

The liquid bridge is formed by a tiny liquid drop that joins the surfaces of spherical steel ball and flat surface. Controlled displacement is given to spherical steel ball by a linear actuator for stretching the liquid bridge and reaction force is continuously measured at the other flat end of the liquid bridge. A cantilever, as a high accuracy force sensor is designed which can measure in the range of μN repulsive or attractive forces. This cantilever is designed with suitable stiffness, strength, and natural frequency to work accurately as a force sensor. This cantilever tip also acts as an interface for liquid bridge one end. Displacement of this tip is measured precisely by a fiber optic displacement sensor. Profile of liquid bridge is acquired digitally during stretching of the liquid bridge for calculation of analytical forces. Computer interface through LabVIEW is developed for controlling linear actuator and acquiring data from the force sensor. Series of experiments are carried out with different stretching rates and three different liquids. Extensional viscosity is calculated by measurement data. Obtained extensional viscosity is compared with reported viscosity data. Analysis of the experimental data is discussed in the result section with estimated forces and viscosity.

CHAPTER-2

2. LITERATURE REVIEW

2.1. INITIAL STUDIES ON LIQUID BRIDGE

Pioneering studies (both experimental and theoretical) of liquid bridges have been undertaken by Plateau, who classified the shapes of the liquid bridges (the surfaces of constant mean curvature) and investigated their stability. The study of the instability of cylindrical fluid interfaces by Plateau was further extended by Rayleigh, who considered also jets of viscous fluid[9].

Liquid bridge, in a static condition, is studied by many researchers. McFarlane and Tabor [10] were the first who started an experimental analysis to carry out a quantitative study of liquid bridge. They studied experimentally the adhesion of spherical beads to a flat plate. They established that in clean dry air the adhesion was negligible. In a humid atmosphere, however, marked adhesion was observed, particularly with hydrophilic glass surfaces. At saturated humidity, the adhesion was the same as that observed if a small drop of water was placed between the surfaces.

2.2. STUDY OF STATIC FORCES IN LIQUID BRIDGE

Theoretical formulas were reported and compared by Yakov et al[11] for the estimation of the capillary force due to a liquid bridge between two spheres with a fixed volume. The distant dependent capillary force was derived theoretically on the basis of two approaches: (1) the total liquid bridge energy and (2) the pressure difference across the liquid bridge (Laplace equation).

Lian et al [12] considered liquid bridges between two spherical rigid bodies of equal radii under conditions where the effects of gravity are negligible. They argued that, at relatively low contact angles, say $<40^\circ$, the critical separation for rupture is given by the cube root of the liquid bridge volume to a good approximation. The toroidal approximation provides a simple method of estimating the total liquid bridge force. The "gorge method" of evaluation leads to errors of $<10\%$ for all stable separations and a wide range of bridge volumes.

Lockwood et al [13] observed the formation of nanoscale liquid droplets by the friction of a solid in real-time. They demonstrated in situ imaging of the moving liquid bridges which strongly interact with the highly mobile nanoparticle debris at the sliding nano-contact. They demonstrated for the first time the formation of a solid-like surface nano-filament creates a two-stage division process of a nano-droplet. They argued that the roughness of the surface where the liquid bridge is formed on a nanometer scale, can significantly alter breakup and produce asymmetric shapes due to the topography of the substrate.

Zhang et al [14], shown the first experimental and theoretical study of dynamic contact angle hysteresis in liquid bridges. They found that the capillary force due to surface tension decreases the dynamic contact angle hysteresis and the viscous force due to the viscosity increases the dynamic contact angle hysteresis.

2.3. DYNAMIC FORCES IN LIQUID BRIDGE

Mazzone et al [15] found experimentally that the strength of the dynamic bridge is dominated by viscous force and not by surface tension and pressure difference forces which govern the strength of the static bridge. They also found that the shape and rupture point of the dynamic bridge is quite different from those of the static case.

Liao et al [16] performed experiments to measure the dynamic properties of wet granular matter in a shear cell device. Their results showed the effect of the liquid bridge force on the dynamic properties is not only dependent on the liquid viscosity but also on the kinetic energy of the granular system.

Crassous et al [17] found that the viscous damping was significantly higher than expected while using surface force apparatus to measure forces exerted between cobalt surfaces by an n-decane liquid bridge formed by capillary condensation.

Pitois et al [18] reported that viscous effects contribute to the increase in the rupture distance, which was found to vary like the square root of the separation velocity.

Shaobiao et al [7] summarized extensive theoretical and simulation study on the liquid bridge. They argued that capillary and viscous forces are largely dependent on the separation distance. An increase in contact angle leads to a decrease in attractive meniscus force but an appreciable increase in repulsive meniscus force but the contact angles have only limited effect on the viscous force.

McKinley et al [8] shown that it is possible to use measurements of the capillary breakup of a viscous Newtonian fluid in order to obtain experimental values for the capillary velocity (that are in quantitative agreement with values determined from rheometry and tensiometry). They investigated the capillary breakup of three Newtonian fluids, glycerol, silicone oil (PDMS) and viscous polybutene oil (PB).

Bozkurt [19] reported the total capillary force exerted by a liquid bridge between two equally-sized glass beads to assess the effects of separation distance, rate of particle separation, the volume of the liquid bridge, and hydrophilicity. They found that the maximum capillary force occurs at nonzero particle separation distance.

2.4. MEASUREMENT TECHNIQUES

Cleveland et al [20] reported that the spring constant of micro-fabricated cantilevers used in scanning force microscopy (SFM) can be determined by measuring their resonant frequencies before and after adding small end masses. They proposed that the spring constant scales with the cube of the unloaded resonant frequency, providing a simple way to estimate the spring constant for less precise work.

The CaBERTM [21] (The capillary breakup extensional rheometer) is a commercially available instrument which provides viscosity, surface tension, elasticity, relaxation time and filament breakup time by the thinning and breakup of a fluid filament.

2.5. THEORETICAL ANALYSIS IN LIQUID BRIDGE

Let us consider an axisymmetric fluid capillary bridge formed between two solid bodies, say sphere and plate as shown in Figure 4. The presence of the capillary bridge will lead to interaction

between these two solid bodies, which can be attractive or repulsive depending on the shape of the bridge. The total axial force, exerted by a liquid bridge, strained between spheres and flat surface, has two components capillary force and viscous force.

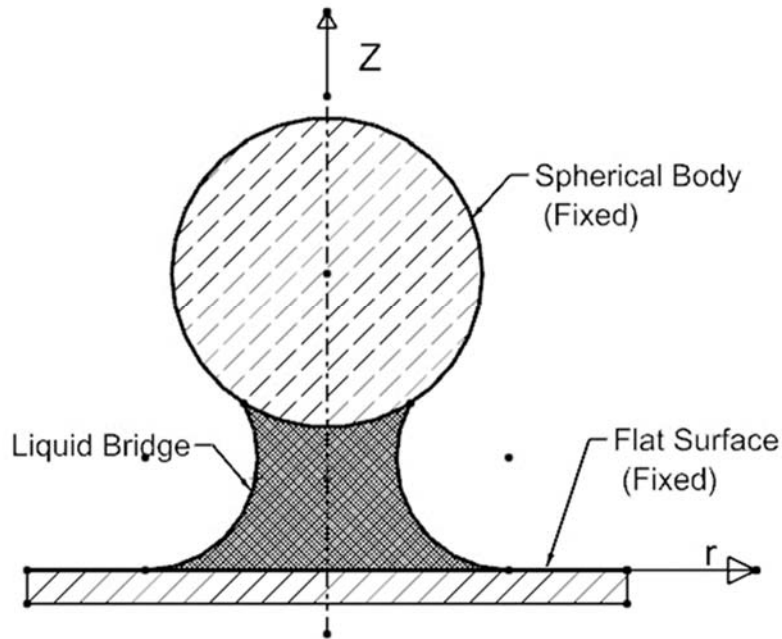


Figure 4: Liquid Bridge between axisymmetric spherical particle and a planar solid surface

Capillary force dominates in the quasi-static regime and viscous forces will be added in dynamic condition with capillary force. So, the effective attractive or repulsive force due to the liquid bridge is a combination of forces due to surface tension, Laplace pressure, and viscosity. Capillary force and viscose force are formulated as below with some assumptions.

$$\text{Total force due to liquid bridge} = \text{Capillary force} + \text{Viscous force} \quad (1)$$

2.5.1. ASSUMPTIONS

Some assumptions are taken for calculation of force considering a liquid bridge forms between two rigid spherical surface and flat surface.

2.5.1.1. DIMENSIONLESS NUMBERS

BOND NUMBER (B_o)

Bond number (B_o) is a dimensionless number; it is defined as the ratio of buoyancy force to surface tension forces. It is used to decide consideration of volume force. If the B_o is less than one, surface forces are dominating and if the bond number is more than one, the gravity force is dominating.

$$B_o = \frac{\Delta\rho L^2}{\sigma} \quad (2A)$$

Here $\Delta\rho$ is density difference, g is gravity, L is characteristic length and σ is surface tension.

CAPILLARY NUMBER

Capillary number (Ca) is a dimensionless number; it is defined as the ratio of viscous stresses and surface tension. The symbol of η is dynamic viscosity and V is characteristic velocity. For low capillary numbers (less than 10^{-5}), flow is dominated by capillary forces whereas for high capillary number the capillary forces are negligible compared to the viscous forces.

$$Ca = \frac{\eta V}{\sigma} \quad (2B)$$

REYNOLDS NUMBER

Reynolds number (Re) is a dimensionless number; it is defined as the ratio of inertial stresses to viscous stresses.

$$Re = \frac{\rho VL}{\eta} \quad (2C)$$

DEBORAH NUMBER

It is a dimensionless number (De); it is the time scale of fluid and time scale of deformation. It quantifies the observation that given enough time even a solid-like material might flow, or a fluid-like material can act solid when it is deformed rapidly enough.

$$De = \frac{t_c}{t_p} \quad (2D)$$

Where symbol 't_c' stands for the relaxation time and symbol 't_p' for the "time of observation", typically taken to be the time scale of the process.

2.5.1.2. NEGLIGIBLE VOLUME FORCE

The assumption for considering small volume, the bond number is less than one, so volume force can be neglected. So, the effect of gravity is not considered in the analysis of the liquid bridge.

2.5.1.3. EQUILIBRIUM STATE

It is assumed that capillary force is calculated at stabilized condition while formulating capillary force.

2.5.1.4. PROFILE OF LIQUID BRIDGE

Rotation symmetry and circular profile of liquid bridge are assumed for geometric analysis for capillary force. Profile of a liquid bridge is assumed as axisymmetric along the Z axis

2.5.2. CAPILLARY FORCES IN LIQUID BRIDGE

Force, due to surface tension, act on the periphery of the intersection of the liquid bridge and solid surface which holds the liquid bridge. The Laplace pressure builds up inside of the liquid bridge, is calculated by the Yong-Laplace equation in the static equilibrium condition. The Laplace pressure act on the projected cross-section area of the liquid bridge in the normal direction at the interface. These two forces, due to surface tension and Laplace pressure, are jointly called *capillary force*. The capillary force acts in both static and dynamic condition.

Capillary force ($F_{cap,n}$), acts in the normal direction (z-axis), is a sum of contributions from the capillary/Laplace pressure ($F_{cap,n,p}$) and the surface tension ($F_{cap,n,\sigma}$) in normal direction as shown in Figure 5. Negative capillary force corresponds to attraction, whereas positive capillary force, corresponds to repulsion between the two bodies. Here, the geometric approach is adopted for calculating the capillary force. Capillary force is balanced in normal direction at the z-axis.

$$F_{\text{cap},n} = F_{\text{cap},n,p} + F_{\text{cap},n,\sigma} \quad (3)$$

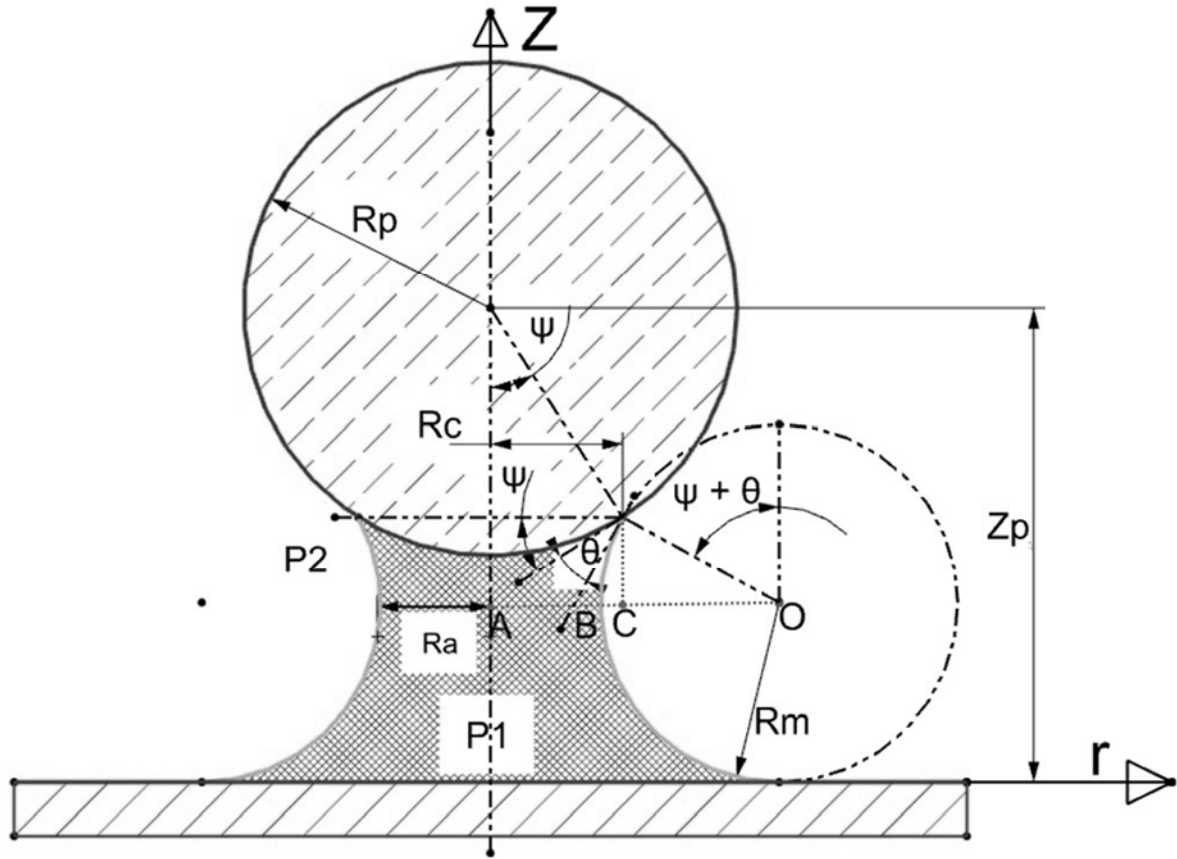


Figure 5: Liquid Bridge configuration

(θ : Contact angle with the sphere, Ψ : Half filling angle, R_p : Sphere radii, R_c : Wetted Sphere radii, R_m : Meridional radii, R_a : Azimuthal radii, P_1 : Inside Pressure, P_2 : Outside Pressure)

2.5.2.1. FORCE DUE TO CAPILLARY PRESSURE

The pressure exhibits a jump on the two sides of a curved interface or membrane of non-zero tension. This effect is quantitatively described by the Laplace equation, which expresses the force balance per unit area of a curved interface. In general, the Laplace equation is a second order nonlinear partial differential equation as given in equation 4 for given Figure 6, a sketch of a two-phase system composed of phase 1 and 2, which occupy volumes V_1 and V_2 , respectively. $z = u(x,y)$ is the equation of the phase boundary, determining the shape of the interface. σ is surface tension, P_1 and P_2 are inside and outside pressures respectively[9].

$$\frac{(1 + u_y^2)u_{xx} - 2u_{xy}u_xu_y + (1 + u_x^2)u_{yy}}{(1 + u_x^2 + u_y^2)^{3/2}} = \frac{[P_2(u) - P_1(u)]}{\sigma} \quad (4)$$

A general form of Young–Laplace equation of capillarity through the two principal radii of curvature of the surface, R_m and R_a is given by relation in equation 5. Where R_m and R_a , are, respectively, the meridional and azimuthal radii of curvature.

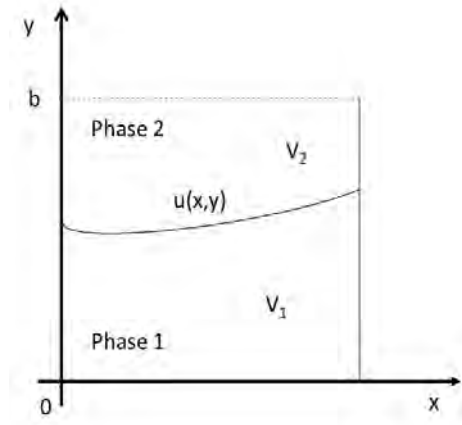


Figure 6: Sketch of a two-phase system composed of phases 1 and 2

$$\sigma \left(\frac{1}{R_m} + \frac{1}{R_a} \right) = [P_1 - P_2] \quad (5)$$

The liquid contact angle is represented by θ , the half filling angle is represented by ψ , R_c represents the radius of that part of the sphere, which is in contact with the liquid. The capillary pressure P_c depends on surface tension as well as the meridional radius R_m and the azimuthal radius R_a , which represents the smallest cross-sectional radius of the liquid bridge: Force due to Capillary Pressure in the normal direction is

$$F_{\text{cap,n,p}} = \pi R_c^2 P_c \quad (6)$$

In accordance with the Laplace equation, the capillary pressure $P_c = P_1 - P_2$ of an axisymmetric meniscus can be expressed as follows:

$$P_c = \sigma \left(\frac{1}{R_m} - \frac{1}{R_a} \right) \quad (7)$$

In general, R_m and R_a vary from point to point and can have a positive or negative sign. The sign convention corresponds to positive R_m and R_a for a sphere.

$$R_a = \begin{cases} R_c + R_m \cdot [\sin(\psi + \theta) - 1] \\ \quad \text{if } \psi + \theta < 90^\circ \\ R_c \quad \text{if } \psi + \theta \geq 90^\circ \end{cases} \quad (8)$$

$$R_m = \frac{Z_p - R_p \cdot \cos \psi}{1 + \cos(\psi + \theta)} \quad (9)$$

2.5.2.2. FORCE DUE TO SURFACE TENSION

The surface tension force is defined as the product of the length of the contact line and surface tension. The normal component of surface tension force will act on the periphery of the intersection of the liquid bridge and solid surface which holds the liquid bridge. A negative sign represents an attractive force between solid surfaces.

$$F_{(cap,n,\sigma)} = -2\pi\sigma R_c \sin(\psi + \theta). \quad (10)$$

2.5.2.3. TOTAL CAPILLARY FORCE IN LIQUID BRIDGE

By substituting forces due to surface tension and force due to the pressure difference

$$F_{cap,n} = -2\pi\sigma R_c \sin(\psi + \theta) + \pi R_c^2 \sigma \left(\frac{1}{R_m} - \frac{1}{R_a} \right) \quad (11)$$

Substituting R_m and R_a in the above relation, assuming $(\psi + \theta) < 0$.

$$F_{cap,n} = -\pi\sigma R_c \left\{ 2 \cdot \sin(\psi + \theta) - R_c \left(\frac{1 + \cos(\psi + \theta)}{Z_p - R_p \cdot \cos \psi} - \frac{1}{R_c + R_m \cdot [\sin(\psi + \theta) - 1]} \right) \right\} \quad (12)$$

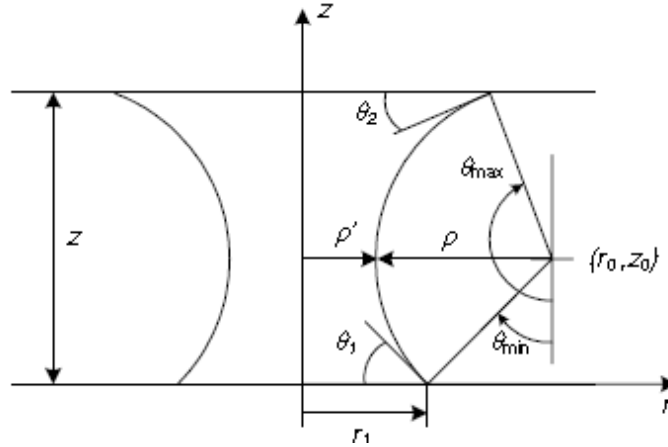


Figure 7: Capillary force with constant volume approach [22]

2.5.3. CAPILLARY FORCE BY CONSTANT VOLUME APPROACH

With this approach, capillary forces can be computed by the assumption of a constant volume of the liquid bridge and the expression is given by below expression for shown in Figure 7 [22]. This force expression is applicable only when the liquid bridge is in stable condition during a stretching regime.

$$F = \pi\sigma r_1^2 \left(\sqrt{\frac{\pi z}{V}} - \frac{\cos \theta_1 + \cos \theta_2}{z} \right) + 2\pi\sigma r_1 \sin \theta_1 \quad (13)$$

2.5.4. VISCOUS FORCE IN LIQUID BRIDGE

When the liquid bridge is extended with some stretch rate, the viscosity of liquid plays its role, an additional viscous force is added with capillary force during dynamic loading where stretching of liquid bridge happens in finite time. In general, the magnitude of the viscous force is much higher than the capillary force. If the stretch rate is very small, the viscous force can be neglected but it can't be neglected always.

So, the formulation of viscous forces during extension is very much essential for the characterization of a liquid bridge. The pressure inside the liquid bridge consists of horizontal pressure gradients, whereas the pressure is constant in any vertical plane, inside a liquid bridge. At the outside of a meniscus ring $r = r_b$ (liquid–air interfacial boundary, which is exposed in ambient), $p(r_b) = p_b$, the ambient pressure. Reynolds ‘lubrication equation with a cylindrical coordinate system is given by Hocking[23]. Where D is the distance between surfaces (spherical ball and flat surface) and $H(r)$ meniscus height at radius r ,

$$\frac{\partial}{\partial r} \left(r H^3(r) \frac{\partial p}{\partial r} \right) = 12 \eta r \frac{\partial D}{\partial t} \quad (14)$$

$$D = Z_p - R_p \quad (15)$$

$$H(r) = D + \frac{r^2}{R_p} \quad (16)$$

At the outside boundary $r = r_b$. By integrating the above equation and apply boundary conditions

$$\Delta p = 3 \eta R_p \frac{\partial D}{\partial t} \left(\frac{1}{H^2(r)} - \frac{1}{H^2(r_b)} \right) \quad (17)$$

The viscous force can be calculated by integrating p over the liquid bridge area

$$F_v = -\frac{3}{2} \pi \eta R_p^2 \left[1 - \frac{D}{H(r_b)} \right]^2 \frac{1}{D} \frac{dD}{dt} \quad (18)$$

2.6. MEASUREMENT METHODOLOGY FOR VISCOSITY

The viscosity of a liquid can be measured by stretching a liquid bridge with two approaches. In the first approach radius and time for the depletion of the liquid bridge is recorded and in the second approach, continuous stretching data is recorded i.e. stretch rate, force at end and length of liquid bridge. Both methods are discussed in the next paragraphs.

2.6.1. TROUTON RATIO

Early experiments of Trouton [24] on uniaxial elongation by stretching a fiber or a filament of liquid and subsequent studies confirmed that at low elongation rates, the elongational viscosity η_e was three times the corresponding shear viscosity η_s , and the ratio of the two values is called the Trouton ratio. Trouton ratio (T_r) is defined as the ratio of elongation viscosity (η_e) and shear viscosity (η_s).

$$T_r = \frac{\eta_e}{\eta_s} \quad (19)$$

For very slow stretching rate, Trouton ratio remains three but for higher stretching rate, this ratio also increases[2]. The values of T_r as large as 1000 have been documented in the literature for visco-elastic shear-thinning fluids. In other words, such a fluid thins in shear but thickens in tension (strain hardening).

2.6.2. FIRST METHODOLOGY FOR VISCOSITY MEASUREMENT

In this methodology, a liquid bridge is stretched between two rigid surfaces. After stretching of the liquid bridge, rigid surfaces are kept stationary. The liquid bridge takes a cylindrical profile after some time. Midpoint radius of this cylinder and time is recorded. Automatically thinning of filament happens and after some time, this capillary bridge collapses. This time is also recorded.

Measurements of the midpoint radius of liquid cylindrical filament and using a simple relation enables to obtain quantitative values for the Newtonian viscosity for a range of viscous fluids. For a Newtonian fluid of viscosity (η_s) and surface tension (σ), time (t), a local force balance, and elimination of the fluid pressure lead to the following evolution equation for the midpoint radius R_{mid} [8]:

$$3\eta_s \left(-\frac{2}{R_{mid}} \frac{d R_{mid}(t)}{dt} \right) = \frac{\sigma}{R_{mid}(t)} \quad (20)$$

The total longitudinal stress along the fluid thread is always assumed to be zero since the column is connected to large quasi-static fluid reservoirs which are themselves attached to the rigid

endplates of the device. Integration of the above equation leads to a linearly decreasing profile which can be written

$$R_{mid}(t) = R_1 - \frac{\sigma}{6\eta_s} t \quad (21)$$

Where R_1 is the initial radius of the thread at time $t = 0$.

$$R_{mid}(t) = \frac{\sigma}{6\eta_s} (t_c - t) \quad (22)$$

t_c is the critical time of the breakup event, which can be determined directly by the initial conditions to be $t_c = 6\eta_s R_1 / \sigma$.

$$\eta_s = \frac{\sigma}{6R_{mid}(t)} (t_c - t) \quad (23)$$

This expression is applicable at the last point of stretching of the liquid bridge when liquid bridge take shape of a cylinder and it is not stable during this regime.

2.6.3. SECOND METHODOLOGY FOR VISCOSITY MEASUREMENT

In this methodology, a liquid bridge is formed between two solid surfaces. This liquid bridge is stretched for measuring the extensional viscosity with a constant stretch rate. Elongation rate, length of liquid bridge and force developed are continuously measured. The elongation viscosity[2] is derived below. Here, T_{zz} is total stress in the axial direction, ' T_{rr} ' is total stress in the radial direction, ' F ' is an axial force, ' A ' & ' r ' are liquid bridge area and radius, Z is the distance from one liquid bridge end, σ is surface tension, $\dot{\epsilon}$ is stretch rate and η_e is extensional viscosity.

$$T_{zz} = \frac{F}{A} - \rho g z - \frac{2\sigma}{r} \quad (24)$$

$$T_{rr} = -\frac{\sigma}{r} \quad (25)$$

$$\eta_e = \frac{(T_{zz} - T_{rr})}{\dot{\epsilon}} \quad (26)$$

For the constant volume of the liquid bridge, the first derivative of volume will be

$$\frac{2}{r} \frac{dr}{dt} + \frac{1}{l} \frac{dl}{dt} = 0 \quad (27)$$

Stretch rate is defined as

$$\dot{\epsilon} = \frac{1}{l} \frac{dl}{dt} = -\frac{2}{r} \frac{dr}{dt} \quad (28)$$

So extensional viscosity, with negligible gravity effect, can be expressed as

$$\eta_e = \frac{\left(\frac{F}{A} - \frac{\sigma}{r}\right)}{\frac{1}{l} \frac{dl}{dt}} = \frac{\left(\frac{F}{A} - \frac{\sigma}{r}\right)}{-\frac{2}{r} \frac{dr}{dt}} \quad (29)$$

With the above relation, for measuring extensional viscosity, we need to measure the force (F) develop at a filament radius (r) and rate of change in radius at that moment. 'A' is an area of filament and σ is surface tension of liquid bridge respectably.

2.7. MEASUREMENT OF CANTILEVER STIFFNESS BY ADDED MASS

The spring constant of cantilevers can be determined by measuring their resonant frequencies before and after adding small end masses. These masses adhere naturally and can be easily removed before using the cantilever, making the method nondestructive [20].

The spring constant of an end-loaded cantilevered beam of the rectangular cross-section is given by

$$k = \frac{(Et^3w)}{4l^3} \quad (30)$$

Where E is the elastic modulus, t is the thickness, w is the width, and l is the length. The beam can be approximated as a spring of stiffness k with an effective mass dependent on the beam geometry. For a uniform-cantilever of the rectangular cross-section, this effective mass is $m^* = 0.24 m_b$ where m_b is the mass of the beam. When an end mass M is added, the resonant frequency is given by

$$v = \frac{\omega}{2\pi} = \frac{1}{2\pi} \sqrt{\frac{k}{M + m^*}} \quad (31)$$

Above equation can be rearranged by

$$M = k(2\pi v)^{-2} - m^* \quad (32)$$

$$\frac{1}{(2\pi v)^2} = \left(\frac{1}{k}\right)M - \frac{m^*}{k}$$

Above equation shows that if several known end masses are added to a cantilever and the new resonance frequencies are measured, a linear plot of added mass versus $(2\pi v)^{-2}$ should give a straight line, the slope being the reciprocal of spring constant.

CHAPTER 3

3. DEVELOPMENT OF EXPERIMENTAL SETUP

For measurement viscosity through stretching of a liquid bridge, an experimental setup is conceptualised. This setup is designed for addressing needs of forming and stretching of a liquid drop and measuring reaction force due to stretching at μN magnitude.

The schematic, shown in Figure 3, is an experimental setup for liquid bridge formation and measurement of force. This setup has the provision of linear actuation with $0.38\ \mu\text{m}$ resolution control for stretching liquid drop. A force sensor is used for a double role which provides support to the liquid bridge as well as to measure reaction force in μN resolution while stretching. Controlling of linear actuator and recording force data simultaneously with a high sample rate is achieved for this experiment. High definition, high frame rate, a digital camera is used for measuring the profile of liquid bridge during extension.

A detailed description of each subsystem used for this experimental setup is discussed in the following paragraphs.

3.1. FORCE MEASURING SUBSYSTEM FOR LIQUID BRIDGE

3.1.1. DESIGN OF FORCE SENSOR

A force sensor is required to measure force developed at another end of the liquid bridge while the liquid bridge is stretched at another side. This force sensor shall be sensitive enough for measuring forces in the resolution of μN force. Force can be sensed by measuring the displacement caused by elastic deformation induced by the loading of an elastic structure. A cantilever beam is an appropriate choice which can be used to measure force as well as support for the liquid bridge at one end. This cantilever is designed with suitable stiffness, strength, and natural frequency to work precisely and accurately as a force sensor.

Displacement of cantilever tip, during stretching of the bridge, is measured through fiber optic displacement sensor, as explained in section 3.1.2. Cantilever beam has a very small size, so it can

be deflected due to own weight, but this deflection does not actually disturb the measurement because deflections due to own weight are restricted to be small. Consequently, the linearity and the superposition principle can be applied, and the own deflection neglected.

Design input parameter for cantilever depends on the range of force to be measured and the maximum resolution of the displacement sensor. Maximum resolution of displacement sensor is depending on the sensitivity of sensor and data acquisition system for measurement of the output voltage of the sensor. The designing parameters of this cantilever are governed by required stiffness, natural frequency and linear elastic limit of the selected material for cantilever. Stiffness of this cantilever is depended on the required minimum force to be measured and resolution limit of displacement sensor.

The lower side of the desired stiffness of cantilever will depend on required minimum force to be measured. For example, silicone oil is taken for capillary force calculation as per the equation is given in chapter 1. Parameters are taken as surface tension 20 mN/m for silicone oil, 1.8 mm diameter steel ball, contact angle 2 degree (will be changed during stretching), half filling angle 5 degrees (depend on initial drop volume), 2.6 mm Z_p (change during stretching). When these values are put in force expression as given in chapter 1, the 1 μ N repulsion force is calculated. Value of this change in force as other parameter is change but mostly it is higher. So, the requirement of a minimum of 1 μ N force can be anticipated.

The sensitivity of displacement sensor, by calibration, comes to approximately 30 mV/ μ m; As per datasheet, sensitivity for this sensor is 45 mV/ μ m. Resolution of output voltage from displacement sensor (measured voltage by data acquisition system with controlled noise by proper earthing) is 1 mV. So, resolution of displacement sensor (Volt/sensitivity, 1 mV / 30 mV/ μ m) is approximately 0.033 μ m. So, stiffness (Minimum force / highest resolution), 1 μ N / 0.033 μ m) comes to near 30 N/m.

Tip diameter of displacement sensor is 3.18 mm, the width of the cantilever shall be more than the width of the cantilever. So, width is fixed to 5 mm. 150 μ m thick sheets of metal are easily available so the thickness of the cantilever is fixed to 150 μ m. The material of the cantilever is selected stainless steel for high strength. Material properties of steel are taken as, density 7800 kg/m³,

Modulus of elasticity 210 G Pa. With these parameters and this relation, Length of the cantilever is calculated to 31 mm.

Natural frequency shall be high to overcome noise in the acquired signal and by using this relation, the natural frequency of the cantilever is calculated as 130 Hz, it is above 50 Hz power supply frequency and much above than required frequency of operations.

The maximum anticipated force to be measured is 3 mN. The bending stress is calculated as 172 M Pa and shear stress is 4.15 K Pa for 0.1 mm deflection for 3mN force. These stresses are lower than the elastic limit of the selected material. So, the designed cantilever will serve the purpose.

The stiffness relation for a cantilever beam, given below is used for calculation

$$K = \frac{3EI}{L^3}$$

Here E symbol is for the Young modulus of the material (Pa), L is the length of the cantilever beam (m) and I refer to the moment of inertia of the cantilever beam section as per following equation

$$I = \frac{bh^3}{12}$$

Here b is thickness and h is the width of the cantilever beam (m). The first undamped natural frequency of this cantilever (rad/s), given below, is used for calculation of natural frequency

$$\omega_n = 1.875^2 \sqrt{\frac{EI}{\rho AL^4}}$$

Here, ρ is density. A is cross-section area of the beam. Bending stresses are calculated by the following relation

$$\text{bending stress} = \frac{My}{I} = \frac{F \cdot L \cdot b/2}{I}$$

Here M is a moment, y is the distance between fiber positions to the neutral axis, and F is a force at the tip of the cantilever. Summary of parameters for designed cantilever is given in the table as followed.

Table 1 Summary of designing parameters for cantilever

Material	Steel	Elastic modulus (E)	210 G Pa	Density (ρ)	7800 kg/m ³
Width (b)	5 mm	Thickness (h)	0.15 mm	Length (L)	31 mm
Natural Frequency (ω_n)	130 Hz	Bending Stress	172 MPa	Stiffness(K)	~30 N/m

3.1.1.1. FABRICATION OF CANTILEVER

For better results and accuracy, the cantilever is cut by wire EDM, so residual stresses shall not develop during fabrication. The fixed end is modified to overcome end effect as shown in drawing of Figure 8. The material selected is stainless steel for this cantilever.

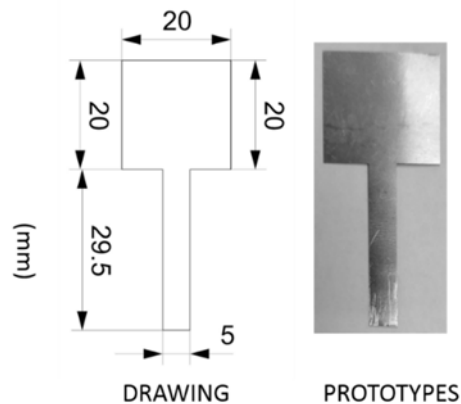


Figure 8: Drawing & Prototypes of Cantilever

3.1.1.2. CALIBRATION OF CANTILEVER STIFFNESS

Stiffness of cantilever is calibrated by measuring natural frequency with different added mass as theory is discussed in paragraph 2.7. Various small pieces of metal were cut, and weight of these pieces is measured in analytical balance, model HTR-220e, M/s Shinko Denshi co ltd. The cantilever is mounted horizontal position for supporting these added masses. These pieces are kept at the tip of the cantilever. A small excitation force is given to cantilever and deflection of the tip is measured by fiber optic sensor with 5000 sample per second rate. Natural frequency is measured by averaging the time required for 20 cycle's deflection. Simultaneously, the natural frequency is also measured by the FFT plot. The plot between added mass and $1/(2\pi\nu)^2$ is shown in Figure 9. Symbol ν is for natural frequency of cantilever with added mass at the tip. By taking linear curve fitting, the slope of the line is 28.66. So, the calibrated stiffness of cantilever is 28.66 N/mm

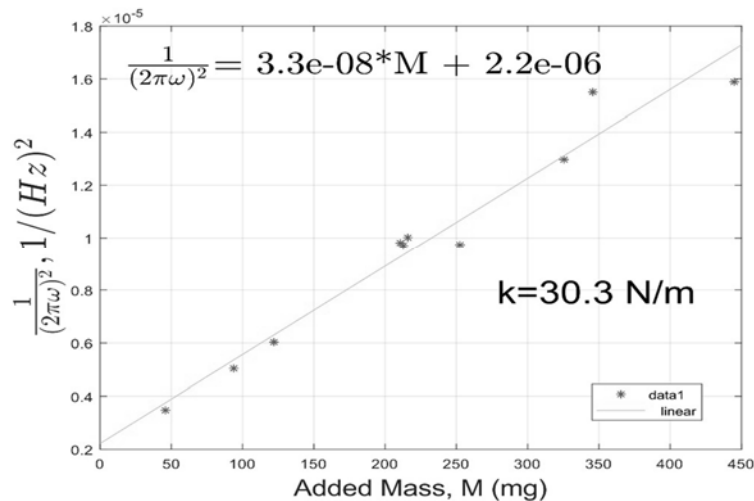


Figure 9: Plot between added mass (M) and $1/(2\pi\nu)^2$ for cantilever calibration

3.1.2. DISPLACEMENT MEASUREMENT SUBSYSTEM

3.1.2.1. DISPLACEMENT SENSOR

To fulfil the objective of assigned work, static and dynamic forces, generated at ends of the liquid bridge, need to be measured. A fixed ended, point loaded, the cantilever is selected for this purpose. The deflection of this cantilever tip is required to measure very precisely with the high-frequency operation.

The fiber optic displacement sensor is most suitable than another sensor like strain gauge sensor which can provide sensing in Nanometer resolution without affecting the performance of the test object. The first selected displacement sensor is Model, DMS D64, Make, Philtec which is non-contact fiberoptic reflectance displacement sensor based upon detecting the intensity of reflected light. The output is proportional to the distance between the sensor tip and target and the reflectivity of the target surface. The change in intensity of light due to the displacement of the target is converted in equivalent voltage output and this is divided by sensitivity for getting displacement. D Models is used where the target reflectivity stays constant and the target has reciprocating motion. Performance of this type of sensor is given in two regions, Far and Near sides. It provides 6 mm total operating range with 1.3 mV/ μm sensitivity, 0.13 μm resolution with 100 Hz, 1.3 mm linear range, 5.8 mm total range for Far side and 45 mV/ μm sensitivity, 8 nm resolution with 100 Hz, 38 μm linear range, 250 μm total range for Near side in best performance conditions[25].

This sensor needs to be calibrated at worktable for getting actual sensitivity. A LabVIEW data acquisition interface was prepared during project work for acquiring voltage output from the displacement sensor. An experimental setup shown in Figure 10, was arranged for calibration of this sensor. The tip of the displacement sensor was clamped on the worktable and one target surface having a reflective surface, is mounted on the XY stage. The output from the sensor is measured through data acquisition interface by NI-9215, C Series voltage input module, with ± 10 V signal range, 50 k S/s sample rate, 12 Bit resolution. A LabVIEW program is developed for recording voltage output from the displacement sensor as explained in 3.1.2.2. First, the distance between sensor and target is set by the Micrometer such that maximum voltage output shall be achieved. Below and higher of this distance output voltage decreases. At this point, the gain (fine and coarse settings) was adjusted in the sensor such that maximum voltage set to 5V.

After this, the minimum distance between the sensor tip and target surface is set with the help of the Micrometer such as output voltage reduces up to minimum voltage (0.5 V). After this, the distance between both is increased in steps of 10 μm and voltage output from the sensor is acquired. This process is repeated for three times to get better accuracy. A graph shown in Figure 11, is plotted between the voltage output and displacement. Near side region and Far-side region

is plotted separately as Figure 12 and Figure 13 respectively for finding the linear zone. With this exercise, 1.16 mV/ μm sensitivity for far side and 30.95 mV/ μm sensitivity for near side is estimated. This sensor is used for measuring the displacement of the cantilever for measuring force at one end of the liquid bridge during further experiments.

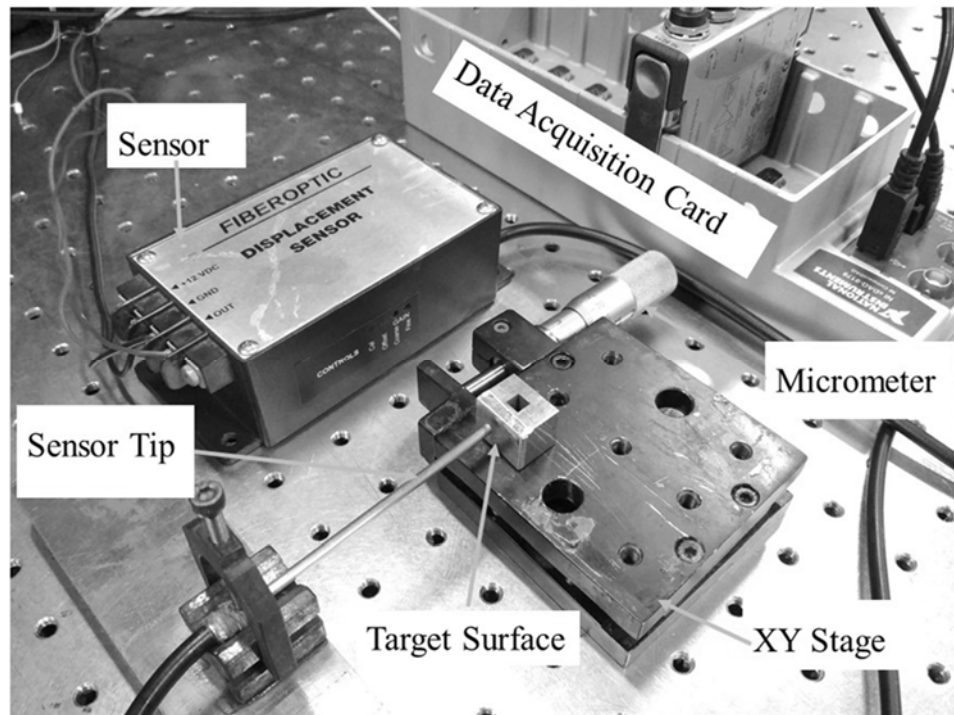


Figure 10: Experimental setup for calibration of Fiberoptic sensor

3.1.2.2. COMPUTER INTERFACE PROGRAM FOR DISPLACEMENT SENSOR

A LabVIEW data acquisition program is developed for acquiring output voltage from the fiber optic displacement sensor for calibration purpose. The output voltage is acquired through NI card with NI chassis. Proper earthing is done to reduce noise in the acquired signal. This signal is acquired as continuous data with a sampling rate of 1024 sample with frequency 1 KHz. The voltage limit was set 0 to 5 Volts for getting higher accuracy. The output voltage is smoothed for 10 points moving average. Low pass filter with 10 Hz to filter white noise and bandpass filter, for noise suppression from 50 Hz power supply, is used. Output displacement is plotted with respect to time. User-friendly interface is developed to acquire the Micrometer reading and sensor output.

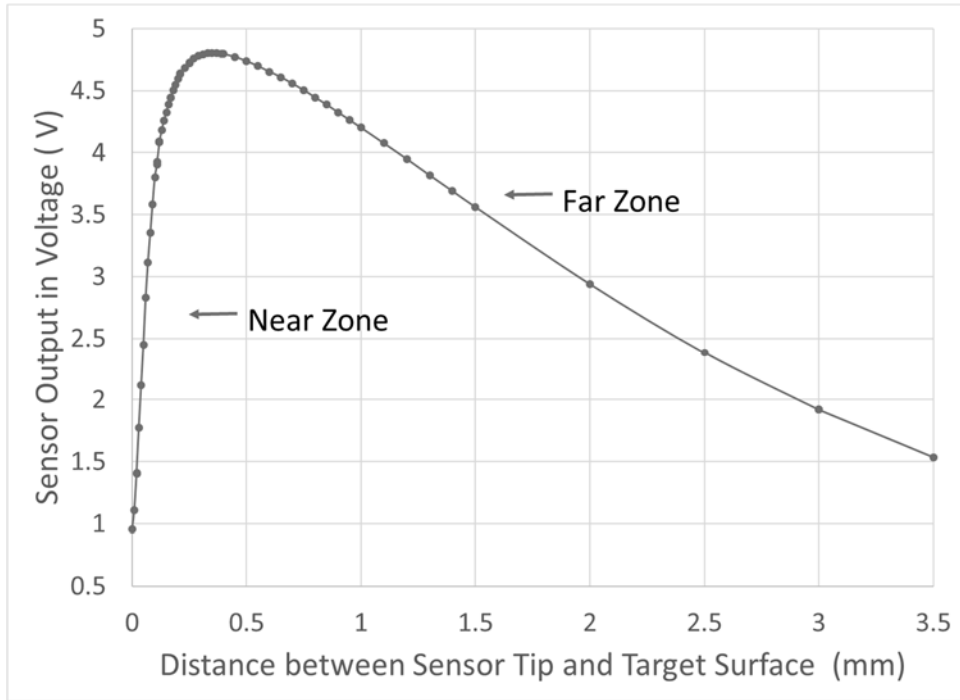


Figure 11: Characteristic of the fiber optic sensor

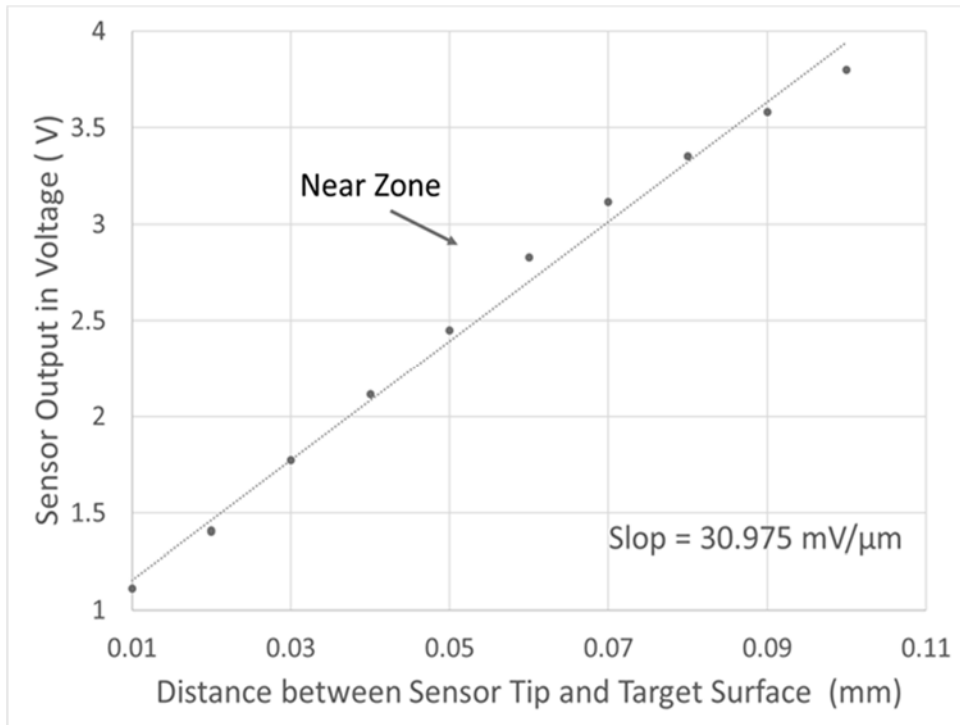


Figure 12: Near side Characteristic of fiberoptic sensor

User needs to first input the initial Micrometer position and step size in the system. Step size and Forward/Backward setting can be altered any time during data acquisition also. After this user needs to press a button to acquire data so Micrometer reading with displacement is recorded in the system. After this system will make increment in Micrometer position. User needs to physically turn the Micrometer and again press button to acquire data. The process is repeated for full bandwidth. This saves the effort of manual typing work. After this user needs to process the data to find a linear region of the sensor.

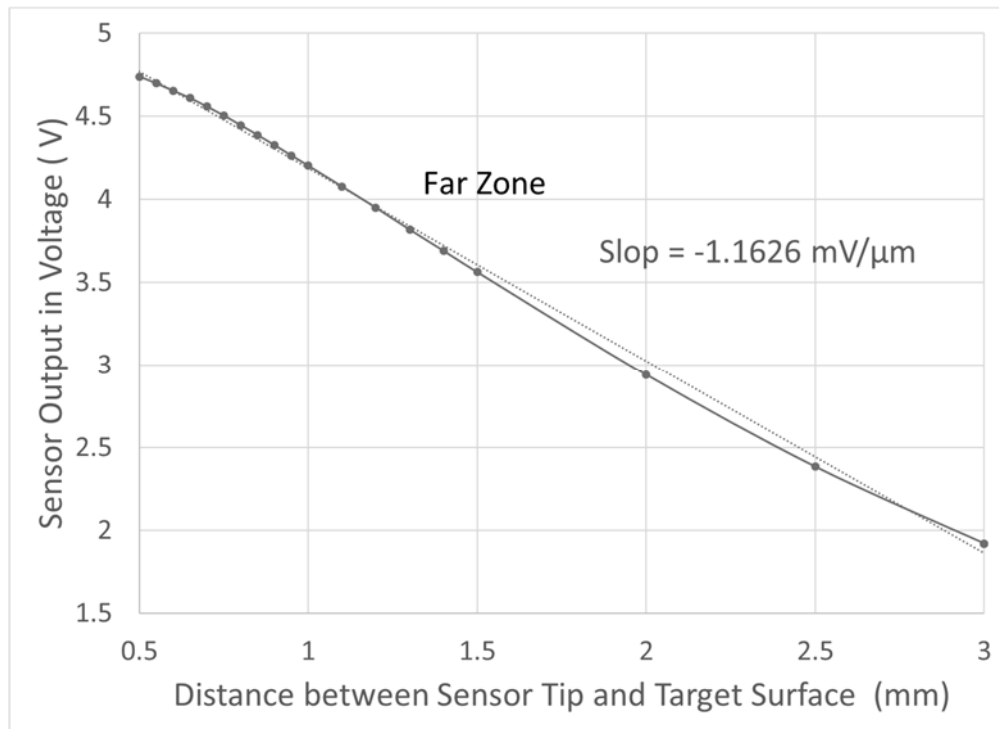


Figure 13: Far side Characteristic of fiberoptic sensor

3.2. IMAGE ACQUISITION SYSTEM

3.2.1. SETUP OF TRINOCULAR WITH INTEGRATION OF USB CAMERA

A digital CMOS camera, Model mvBlueFOX-IGC-205C as shown in Figure 14 is mounted on Trinocular as shown in Figure 15 for acquiring images of liquid bridge digitally. This 5 M pixel camera has resolution of 2592 x 1944, 2.2 μm pixel size, up to 5.8 frame rate and 37.4 max SNR. An additional digital camera is mounted at eye-piece of trinocular for recording high frame

recordings[26]. This setup is useful for carrying out stretching of liquid bridge experiment. It helps to see the forming and breaking of the bridge and measuring dimensions of the bridge for further calculation.

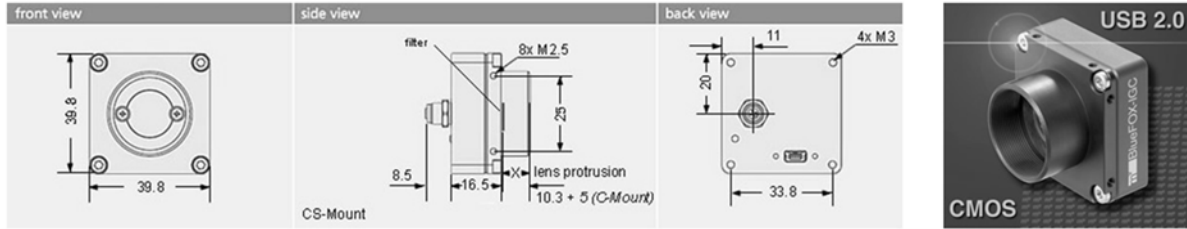


Figure 14: USB Camera (mvBlueFOX-IGC) [27]

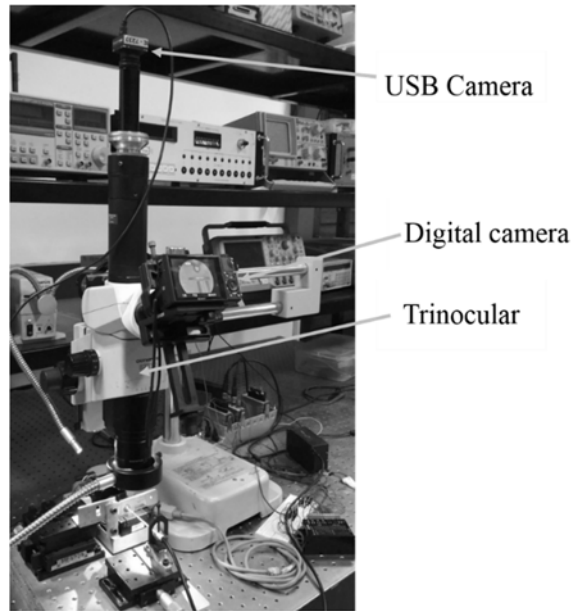


Figure 15: Assembly of Trinocular with USB Camera and digital camera

3.3. SUBSYSTEM FOR LINEAR STRETCHING OF LIQUID BRIDGE

3.3.1. LINEAR ACTUATION FOR QUASI-STATIC STRETCHING

3.3.1.1. CHARACTERIZATION OF LINEAR PIEZO POSITIONING SYSTEM

A linear piezo positioning system, Model P-611K125 NanoCube, Make Physik Instrumente (PI), as shown in an experimental setup in Figure 16, is used for precisely controlling the displacement in nano-meters in all three XYZ axis. It has dimension of 44 mm × 44 mm × 44 mm, travel range

of $200\ \mu\text{m} \times 200\ \mu\text{m} \times 200\ \mu\text{m}$ in XYZ directions, resolution up to 2 nm, 15 N push & 10 N pull force capacity in motion direction, stiffness $0.2\ \text{N}/\mu\text{m}$ with vacuum compatibility.

This piezo stage is controlled by E-664 NanoCube Piezo, 3-axis, controller through manually by knobs or externally by 3 analogue BNC input signal. This controller input voltage range for the control signal is -2 to 12 V and the output voltage range are -20 to 120V for the piezo stage. This controller indicates voltage as well as position in μm . Knobs of this controller can only use with steps of $1\ \mu\text{m}$.

This piezo stage with its controller was controlled through an external voltage signal for characterization. Experimental set as shown in Figure 16 was arranged where the position of the piezo stage was measured and recorded as explained in section 3.1.2 through the fiber optic displacement sensor. A voltage signal was generated with the help of NI-9265 C series current output module. This module provides 0 mA to 20 mA current, 16-Bit digital to analogue resolution, 100 K S/s per channel sampling rate. Voltage source was generated across a $600\ \Omega$ resistor by controlling current from NI-9265 module. Output displacement of the piezo stage also can be monitored from E-664 controller in 0 to 10 V signal for all three axis so this signal was recorded with the help of NI-9215, C Series voltage input module. A LabVIEW program was generated for controlling the voltage signal and recording output displacement for characterization of piezo stage as explained in section 3.3.1.2. Signal control and measurement experiment were done for each axis of the piezo stage independently. When input voltage was controlled from 0 to 10 V, the output from the piezo stage was measured from 0 to $200\ \mu\text{m}$ displacement and linear relationship was found between the input voltage and output displacement in all three XYZ axis. This stage is used for stretching the liquid bridge during quasi-static stretching experiments.

3.3.1.2. COMPUTER INTERFACE FOR NANO CUBE CHARACTERIZATION

One input and two output signals are required for characterization of the piezo stage for each axis individually. LabVIEW program was developed for interfacing these signals. Noise cancellation through averaging and bandpass & low pass filters was achieved. This program provides flexibility to the user to opt coarse or fine control of the input signal for the fast or slow movement of the piezo stage.

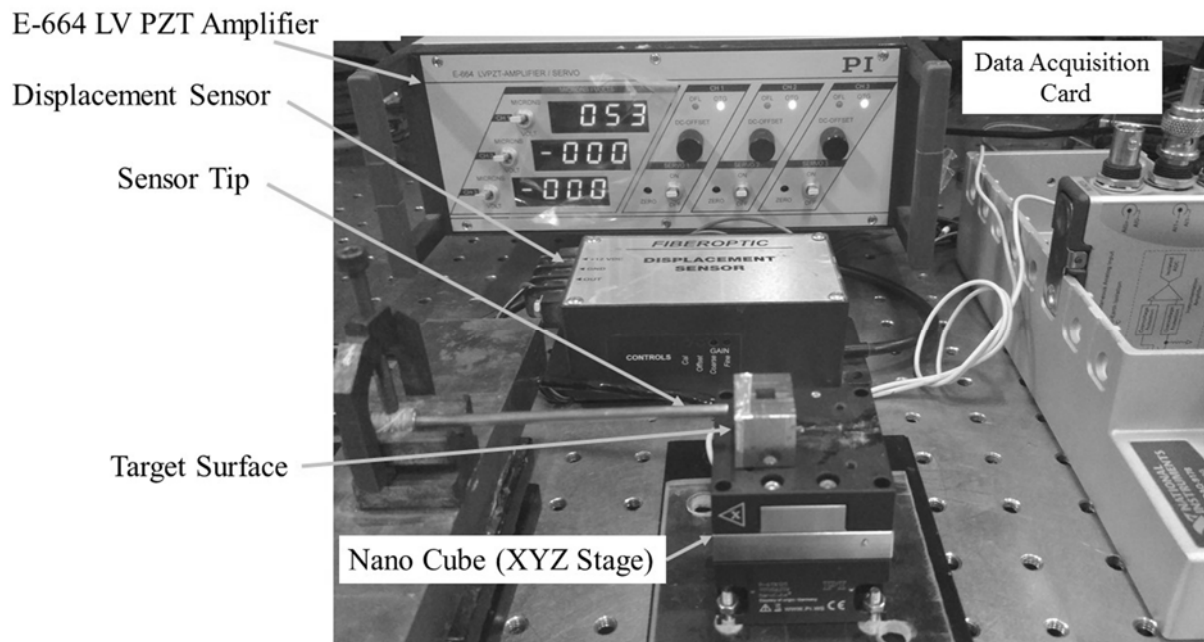


Figure 16: Experimental setup for characterization of Piezo XYZ stage (Nano cube)

3.3.1.3. INTEGRATION OF MICRO STAGE FOR LIQUID BRIDGE

Piezo XYZ stage (nanocube) gives only 200 μm displacement so it is difficult to form the liquid bridge and stretch with the manual stage. To overcome limitation of travel limit, a micro stage, Model M3-LS-1.8-6, Make NewScale, as shown in Figure 17, having size of 29 x 20 x 10 mm, mass of 8.5 grams, stroke of 6 mm, and travel resolution of 0.5 μm and operating force of 0.2 N, added in an experimental setup. This micro stage (for coarse control) is mounted on the XYZ piezo stage (for fine control). It is controlled by software provided by the company separately. With the integration of this, liquid bridge formation and the stretching experiment repeated.

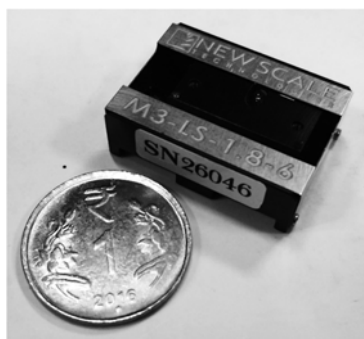


Figure 17: Micro stage, Model M3-LS-1.8-6, Make NewScale

3.3.2. LINEAR ACTUATION FOR CONTINUOUS STRETCHING

Data acquisition for force measurement and control of the travelling stage need to be done simultaneously for continuous stretching operation. Force data acquisition is done through LabVIEW Piezo actuators have a very narrow range in linear motion and micro stage does not provide controlling support with LabVIEW. To overcome this limitation, a stepper motor controlled linear actuator with micro stepping is used with LabVIEW control.

3.3.2.1. STEPPER MOTOR CONTROLLED LINEAR ACTUATOR

A stepper motor with a gear system and lead screw in a linear actuator is used as shown in Figure 18. Gear ratio is 4 and the pitch of the lead screw is $0.38 \mu\text{m}$ for this linear actuator. A micro step controller is used for controlling this stepper motor as shown in Figure 19. The model number of the stepper motor is HY 200 1613 016A6 from M/s Shri Katragadda electronics ltd have the specification of $R 75 \Omega$, class B. Holding torque for this motor is 0.8 Kg-cm (0.078 Nm).

3.3.2.2. DETAILS OF MICROSTEP DRIVER FOR STEPPER MOTOR

A microstep driver is used for controlling the stepper motor for smooth running which is shown in Figure 19.

3.3.2.3. CHARACTERIZATION OF STEPPER MOTOR

Stepper motor is characterized for its motion. The given travel, as shown in Figure 20, gives output displacement as shown in Figure 21. Here vibration level was monitored very high as shown in the right picture of Figure 21. Further excitation force was given to various points in linear actuator and frequency of vibration were monitored to find out the real cause of the vibration. The motor was hanged on the 'L' shaped plate, as shown in Figure 22. The hanging motor was giving vibration. A vibration damper is fixed to restrict the free movement of the motor with the L shaped fixture which reduces vibration. Again motor was given a signal as shown in Figure 20 and output was measured as shown in Figure 23. This output clearly shows the reduction of vibration amplitudes. This improves the efficiency of the system.

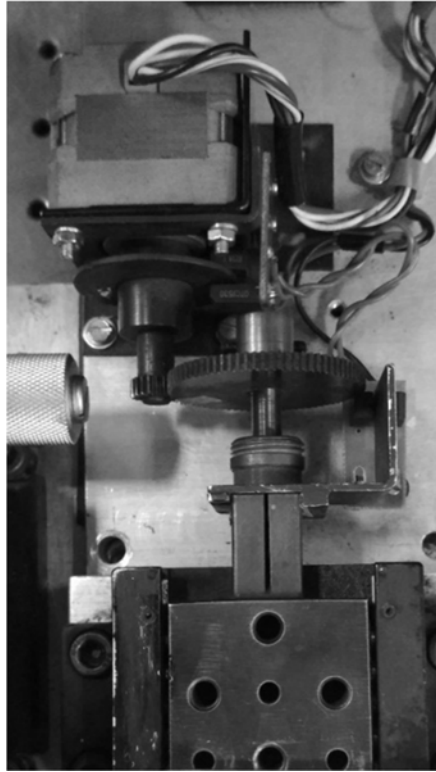


Figure 18: Linear actuator with stepper motor

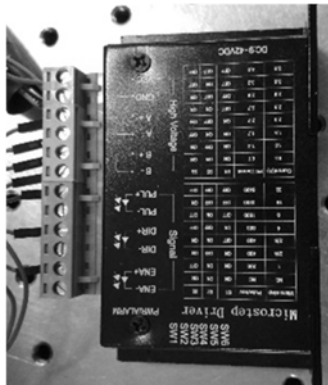


Figure 19: Microstep driver for stepper motor

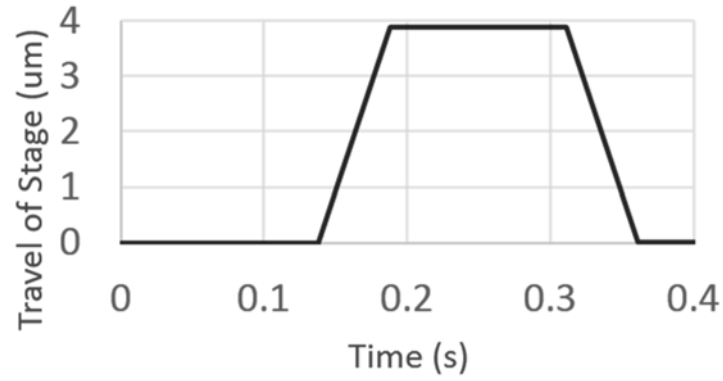


Figure 20: Expected displacement of stepper motor

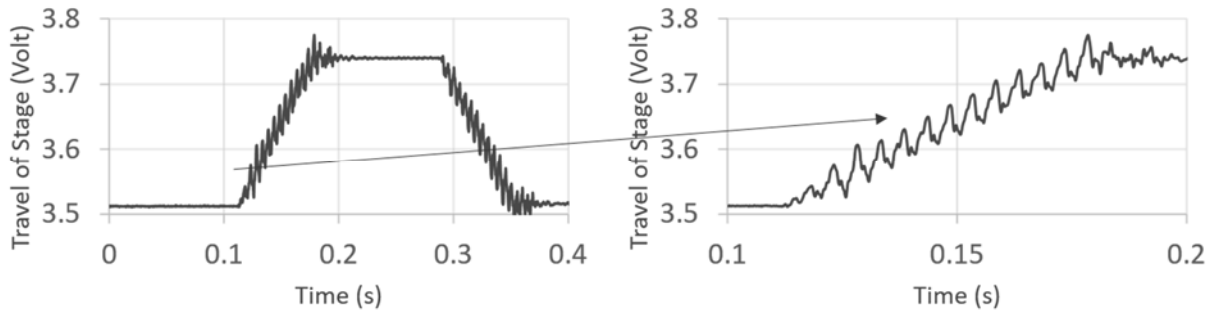


Figure 21: Measured displacement of Stepper motor in Volts before applying damper

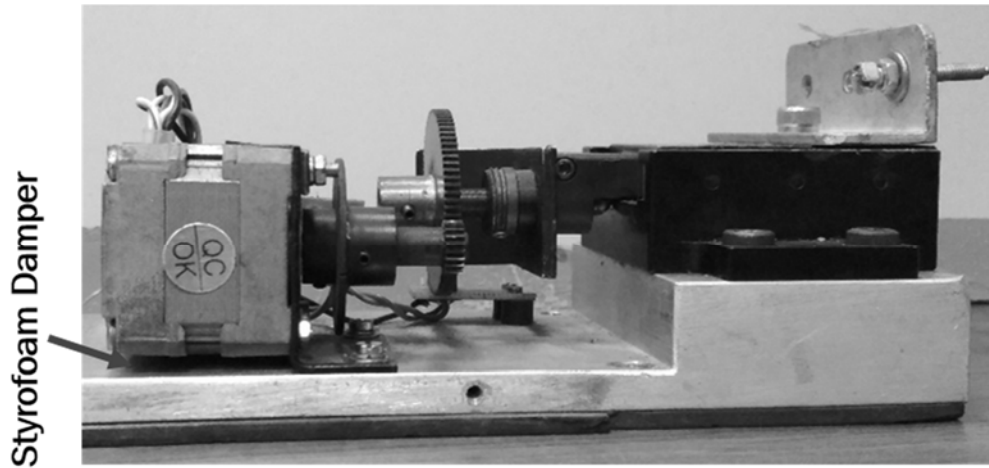


Figure 22: Isolation of vibration from the linear actuator

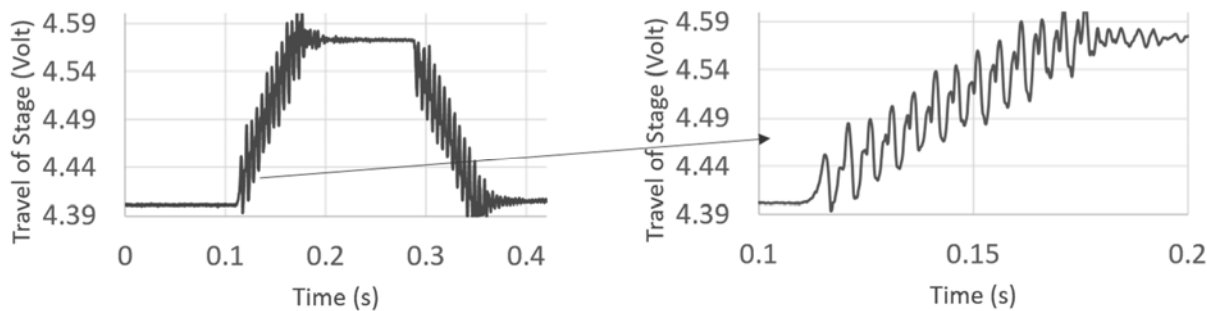


Figure 23: Measured displacement of Stepper motor in Volts after applying damper

3.3.2.4. COMPUTER INTERFACE FOR CONTINUOUS STRETCHING EXPERIMENTS

LabVIEW program is developed for interfacing stepper motor control with micro stepping by PWM (pulse width modulation) by NI card NI9263 and data acquisition with a high sample rate up to 100 k sample per second continuously and simultaneously. The data is recorded in the TDMS (technical data management streaming) format for high-speed rates with simultaneous controlling the stepper motor. This program provides flexibility to the user to control with different speed for specified desired displacement.

3.4. LIQUID SAMPLES

In this work, two types of liquid are used i.e., Silicone oil and DI Water. Properties are listed in below tables.

3.4.1. SILICONE ELASTOMER

Silicone elastomer which is known as PDMS (Polydimethylsiloxane), is used for experiments. The properties are listed in below table

Name of the company	M/s Dow Corning
Product code	Sylgard 184[28]
Chemical formula	$(C_2H_6OSi)_n$
Density	965 kg/m ³
Molecular weight (estimated)	67700 g/mol for viscosity 12 Pa.s (12500 cs) [29]

Viscosity	5.1 Pa.s [28], 10.5 Pa.s [8]
Surface Tension	20.9 mN/m [8], 21.06 mN/m[29]

3.4.2. DI WATER

Liquid Name	Deionized water
Chemical formula	H ₂ O
Density	999.83 kg/m ³
Molecular weight (estimated)	18 g/mol
Viscosity	0.00089 Pa.s
Surface Tension	72 mN/m
Vapour pressure	3.1 kPa at 25 ⁰ C

3.4.3. 1-DODECANETHIOL

Liquid Name	1-DODECANETHIOL
Chemical formula	C ₁₂ H ₂₆ S
Density	0.8 g/cm ³
Molecular weight (estimated)	202.39 g/mol
Viscosity	3.24 mPa.s
Surface Tension	30 mN/m
Vapour Pressure	133 Pa at 48 ⁰ C

CHAPTER 4

4. RESULTS

4.1. QUASI-STATIC STRETCHING OF LIQUID BRIDGE

4.1.1. DETAILS OF EXPERIMENT FOR QUASI-STATIC STRETCHING

A fine control stage (micro stage) was mounted on coarse stage (nanocube) as shown in the experimental setup in Figure 24. During the experiment, a 2.2 mm diameter steel ball was fixed on the micro stage with small fixture and this micro stage was mounted on XYZ piezo stage. This XYZ stage was fixed on the worktable. An initially designed cantilever was mounted on another fixture which was mounted on the worktable. The gap between the steel ball and cantilever was adjusted 4 mm. A fiber optic displacement sensor positioned on the opposite face of the cantilever and it was characterized again. A silicone oil drop was put on cantilever towards the ball side. Displacement, in 10 μm steps, through a computer, was given to micro stage to approach towards silicone drop. Jump in contact was happen when the drop was just near to the cantilever. This was seen through the digital camera on the computer. After this reverse displacement was given to micro stage so the liquid bridge can be stretched. During approaching and stretching, displacement of cantilever displacement was recorded in each step after stabilization. With this displacement and cantilever stiffness, the force was calculated. Some pictures of liquid bridge formation are shown in Figure 25. First two pictures show the approach of the sphere to the flat surface. The third picture shows the ‘jump in contact’. Third, the fourth and fifth picture shows the stretching of the liquid bridge.

4.1.2. FORCE DISPLACEMENT CURVE FOR QUASI-STATIC STRETCHING

A graph between, this force and micro stage travel is plotted as shown in Figure 26 for the quasi-static stretching experiment. When SS ball approaches towards the liquid drop, there is no force, which is shown in graph with a right arrow at zero force. After a jump in contact, force in increased suddenly, this step is shown by a downward arrow with highest negative force. When stretching happens, force decreases, this is shown slanting upward arrow. At break up force become zero, this point also indicated in the graph at zero force line.

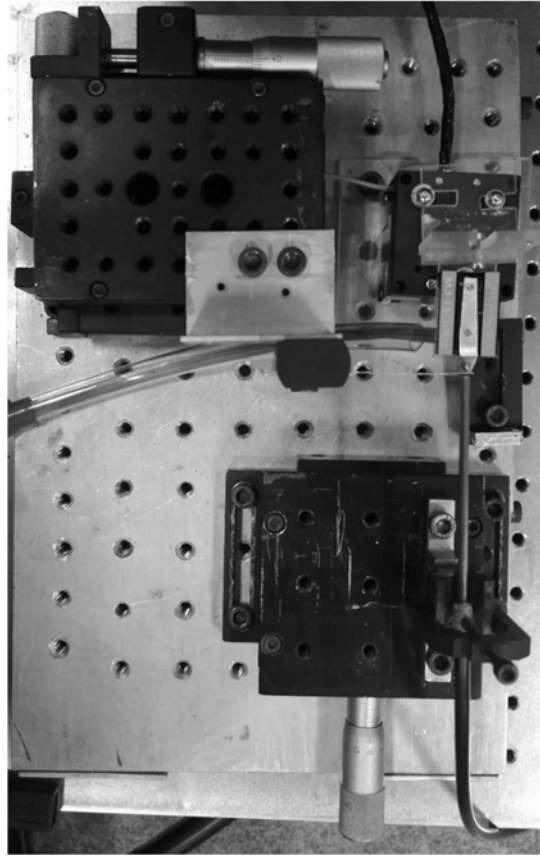


Figure 24: Experiment setup for quasi-static stretching

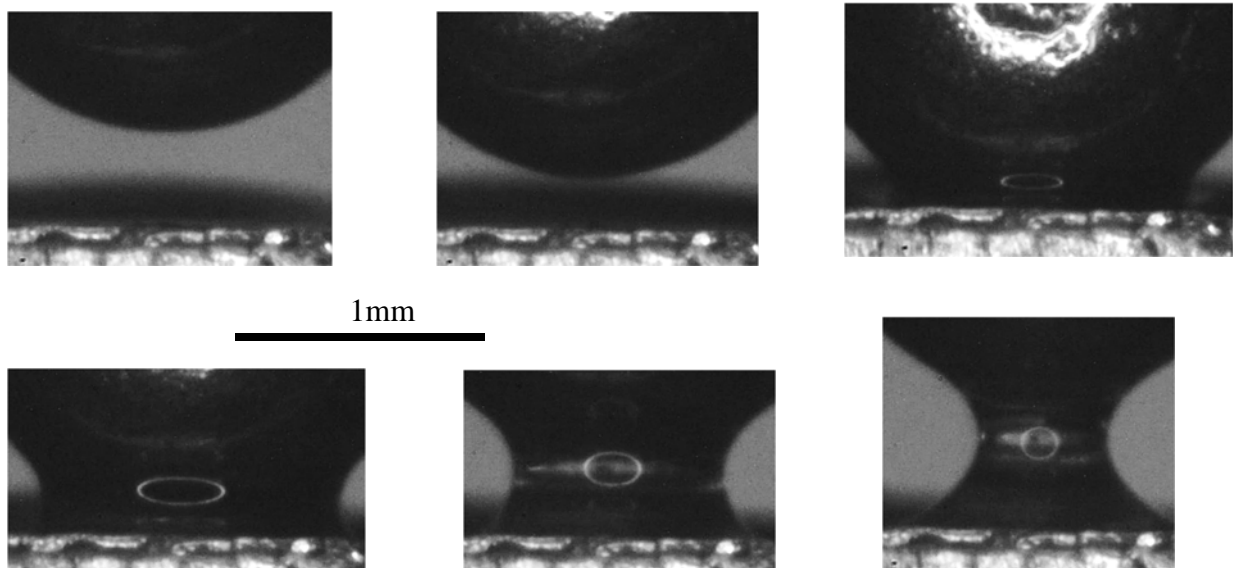


Figure 25: Liquid bridge formation during quasi-static stretching

4.2. EXPERIMENTS WITH CONTINUOUS STRETCHING OF LIQUID BRIDGE

4.2.1. EXPERIMENTAL SETUP FOR CONTINUOUS STRETCHING

Liquid bridge forms between two rigid surfaces of spherical ball and flat thin plate as shown experimental setup in Figure 27. Both surfaces are cleaned by an isopropanol solution before putting a liquid drop. The flat thin plate is a part of the cantilever which acts as a force sensor. Displacement of this cantilever tip, due to stretching of the liquid bridge, is measured by non-contact type fibre optic, reflectance-based displacement sensor. Steel ball act as another rigid spherical surface for the liquid bridge. The displacement of this steel ball is controlled by linear actuators, stepper motor. The resolution of this linear actuator is $0.38 \mu\text{m}$ by using a gear mechanism. The digital images of this liquid bridge are acquired by a USB camera. Controlling and data acquiring simultaneously is done in LabVIEW software. Deflection of the cantilever is recorded at a high sample rate up to 5000 sample per second (S/S).

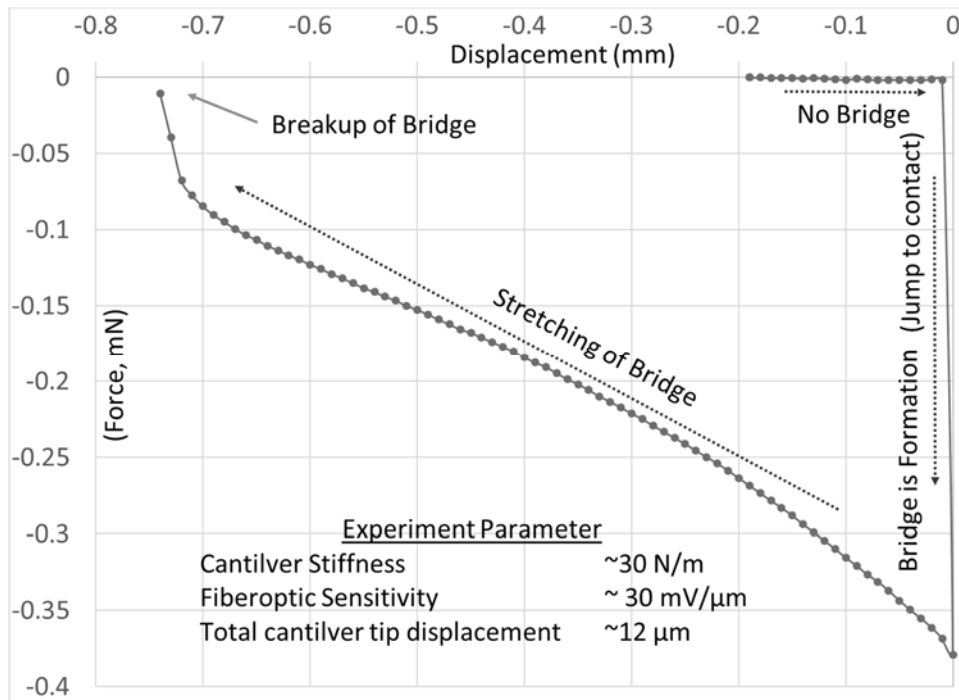


Figure 26: Micro Stage displacement vs Cantilever reaction force for silicone oil drop.

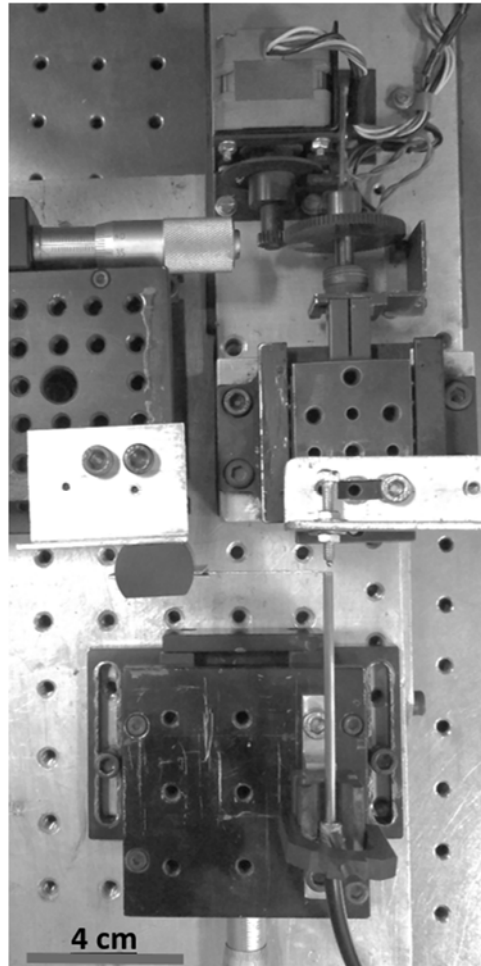


Figure 27: Experimental setup with continuous motion

4.2.2. EXPERIMENT PROCEDURE FOR CONTINUOUS STRETCHING

A liquid drop of liquid (Silicone elastomer, DI water or 1-Dodecanethiol) is placed on tip of cantilever surface. Displacement is given to steel ball by the linear actuator to approach liquid drop with specified speed. This displacement and force are shown in corresponding figures (details are given in para 4.2.2.1 to 4.2.2.3) by the regime- 'A'. There is no reaction force in cantilever, so the force is zero. When the displacement of the sphere, towards cantilever, keeps continuing; after some given travel to a linear actuator, the tip of the cantilever with a liquid drop jumps to contact towards steel ball. A liquid bridge is formed between a steel ball and cantilever. This jump to contact is shown corresponding figures at regime- 'B'. The reaction force increases in cantilever due to negative capillary force for further approaching to cantilever surface. Here force reaches to

the local minimum value. After a certain distance, the reaction force increases, and it reaches to zero, shown corresponding figures at regime- 'C'. At this condition steel ball and cantilever touch each other and there is no deflection in cantilever. So, force becomes zero. Further displacement of steel ball towards cantilever, create penetration effect and cantilever deflect in the opposite direction and positive force in cantilever is developed. This regime is represented shown corresponding figures at regime- 'D'. A predefined delay is given to stop the movement of the linear actuator at this movement. At this point, the liquid takes an equilibrium position by draining towards maximum stability. Now steel ball is reverted, the force is decreased as shown corresponding figures at regime- 'E'. The force becomes maximum after reaching a certain distance as shown in shown corresponding figures. This force reaches global minimum value. Further, stretching of liquid bridge keeps continuing at a fixed stretch rate. Force reduces simultaneously as shown corresponding figures at regime- 'F'. After a certain distance, capillary bridge breaks and cantilever reaction force becomes zero as shown corresponding figures at regime- 'G'.

4.2.2.1. EXPERIMENT WITH SILICONE OIL

Stretching force in silicone elastomer is measured with respect to the length of the liquid bridge with the help of developed experimental setup. Raw data of the force vs displacement curve is shown in Figure 28. This raw data is filtered with 100 points moving average. The snapshot of the jump in the contact portion with raw and filtered data is shown in figure Figure 29. This experiment is repeated with different speeds and results are shown in Figure 30, Figure 31 and Figure 32. The resultant curves of these experiments are superimposed which are shown in Figure 33. This comparison shows that the nature of profiles for each experiment is matched with each experiment with the same liquid. This comparison also indicates, jump in contact point moves forward with each repeated experiment. This can be due to draining of silicone oil from the surface of the cantilever. Further, this less quantity also may be responsible for changing the magnitude of the maximum attractive force. Force vs time for silicone is plotted in Figure 34. This curve helps to recognise the effect of delay time between forwarding and backward motion. Here, the effect of draining of liquid towards the ball, while the actuator is not moving during delay time, changes the reaction force. This slow decay of force without stretching of the liquid bridge with respect to time can be utilised for calculation of viscosity.

Various regimes of stretching of silicone elastomer are represented in force vs displacement curve and force vs time curve as shown in Figure 30 and Figure 34 respectively. Explanation of regimes is given at paragraph 4.2.2. Pictures of these regimes for silicone is shown in Figure 35. Here regime ‘A’ shows approaching the ball towards silicone drop held at cantilever tip. At regime ‘B’ jump in contact happens and attractive force in silicone liquid bridge reached up to $-80 \mu\text{N}$. Regime ‘C’ shows further penetration of ball in silicone drop. At regime ‘D’, the positive force reached up to $300 \mu\text{N}$. At regime ‘E’, the formation of silicone liquid bridge, where attractive force increases as stretching increases. After achieving a maximum attractive force of $-620 \mu\text{N}$, regime ‘F’ starts. In this regime, the attractive force decreases sharply. The neck portion of the silicone liquid bridge takes concave shape at this regime. The force is exponential decay at this regime.

Finally, the liquid bridge takes a cylindrical shape and at this stage, viscous force dominates on capillary forces. This regime is generally utilised for measurement of viscosity of the subjected liquid. This regime is marked as ‘G’. Extensional viscosity is measured from this regime which is discussed in paragraph 4.3.

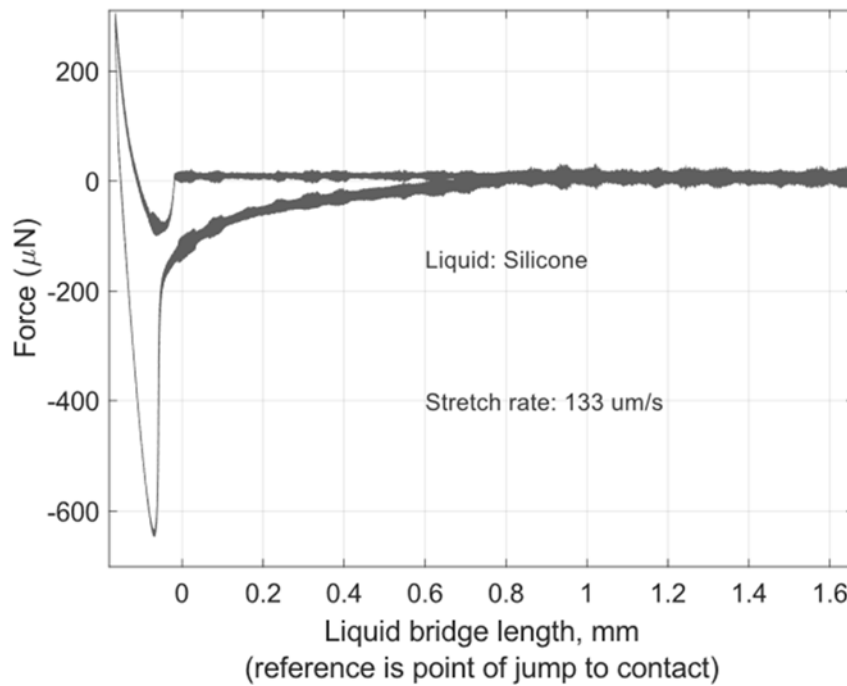


Figure 28: Force vs displacement curve with Raw data for silicone elastomer with a stretch rate of $133 \mu\text{m/s}$

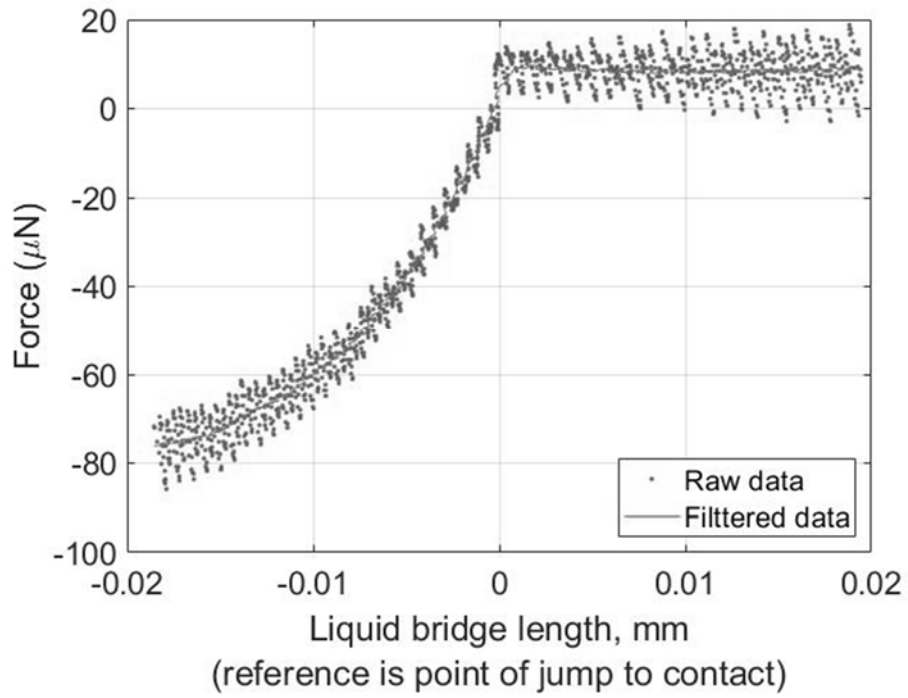


Figure 29: Raw data is filtered with 100 points moving average (snapshot of data at the jump in contact) for silicone

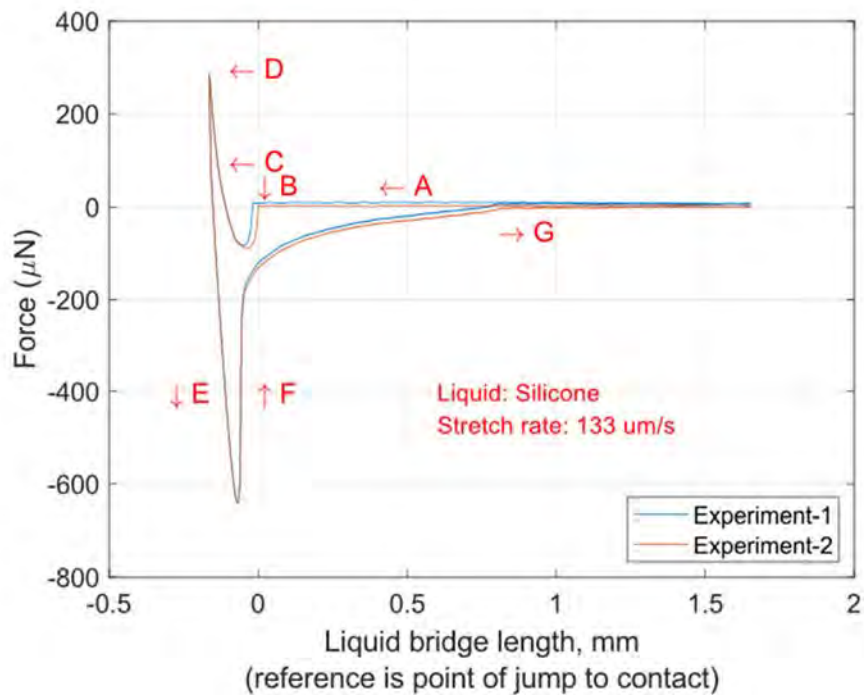


Figure 30: Filtered force vs displacement curve for silicone with a stretch rate of 133 $\mu\text{m/s}$

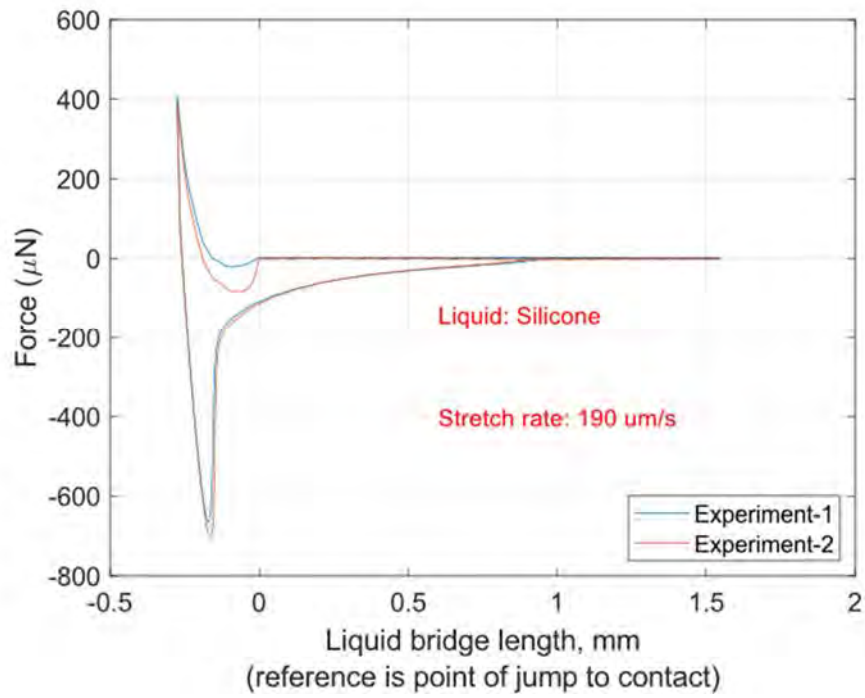


Figure 31: Filtered force vs displacement curve for silicone with a stretch rate of $190 \mu\text{m/s}$

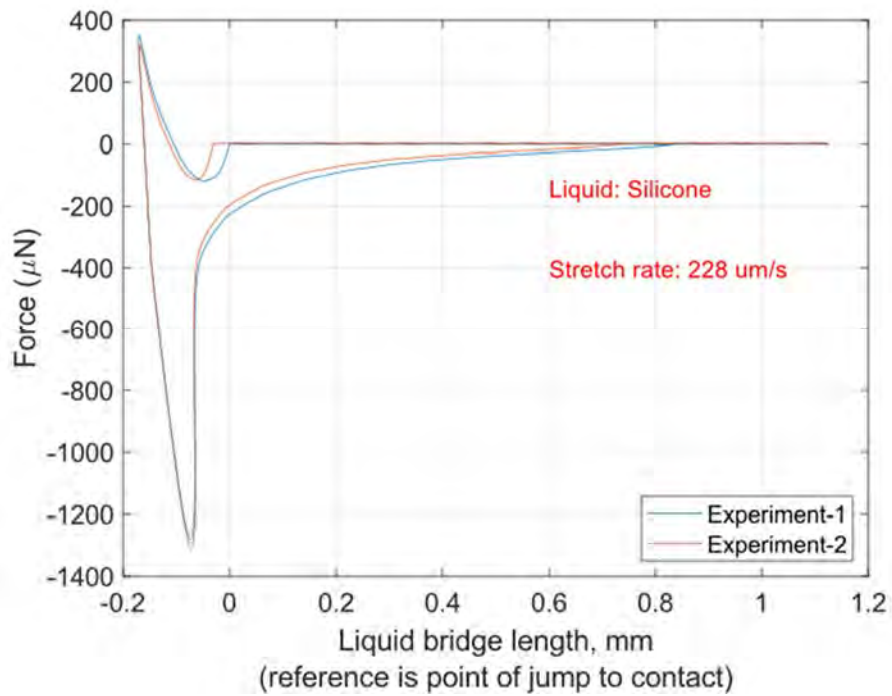


Figure 32: Filtered force vs displacement curve for silicone with a stretch rate of $228 \mu\text{m/s}$

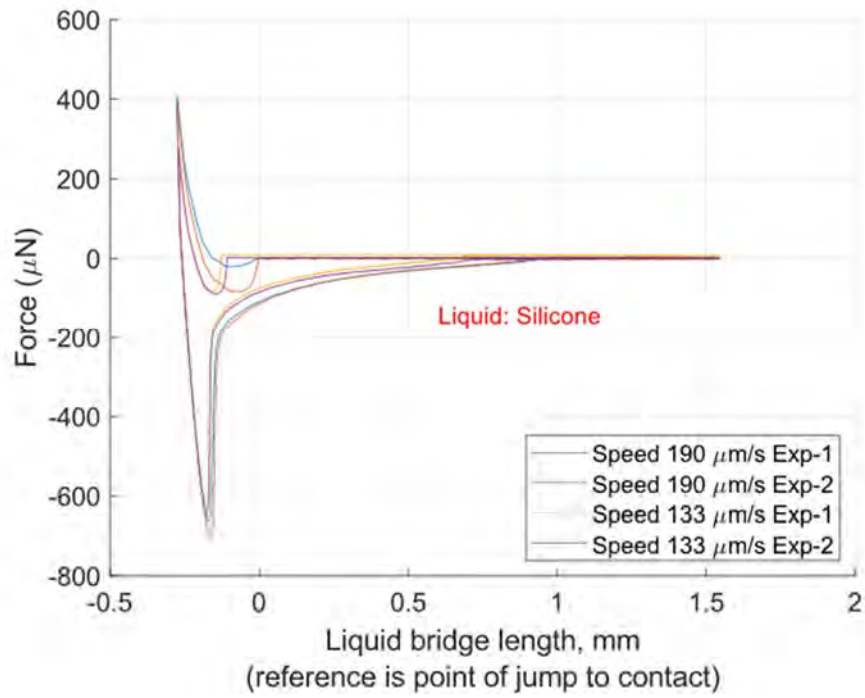


Figure 33: Compare force vs displacement curve for silicone with the different stretch rates

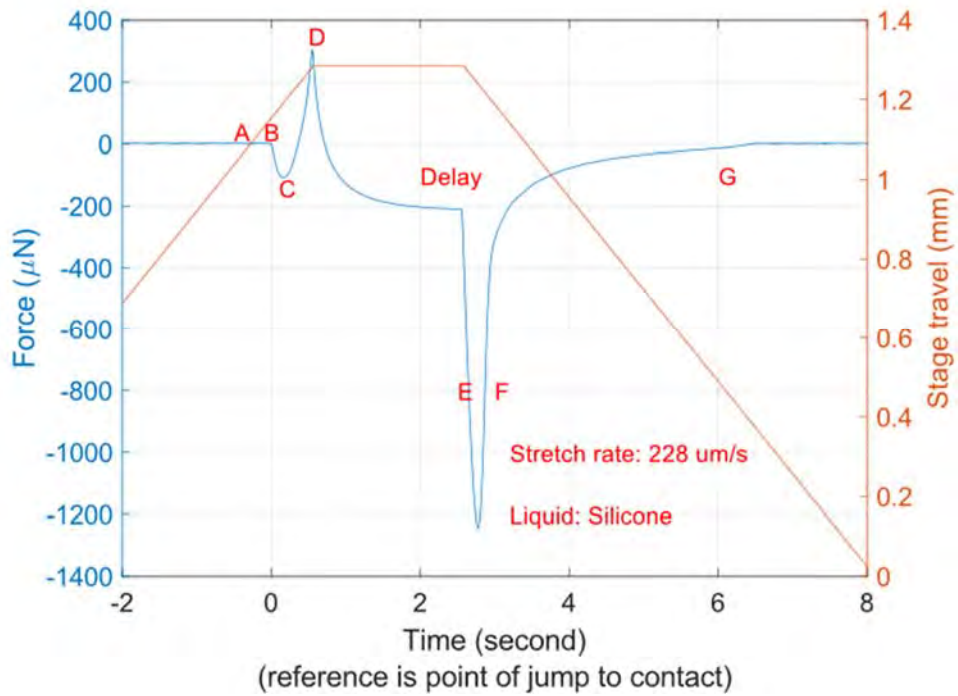


Figure 34: Filtered force vs time curve for silicone elastomer with a stretch rate of 228 $\mu\text{m/s}$

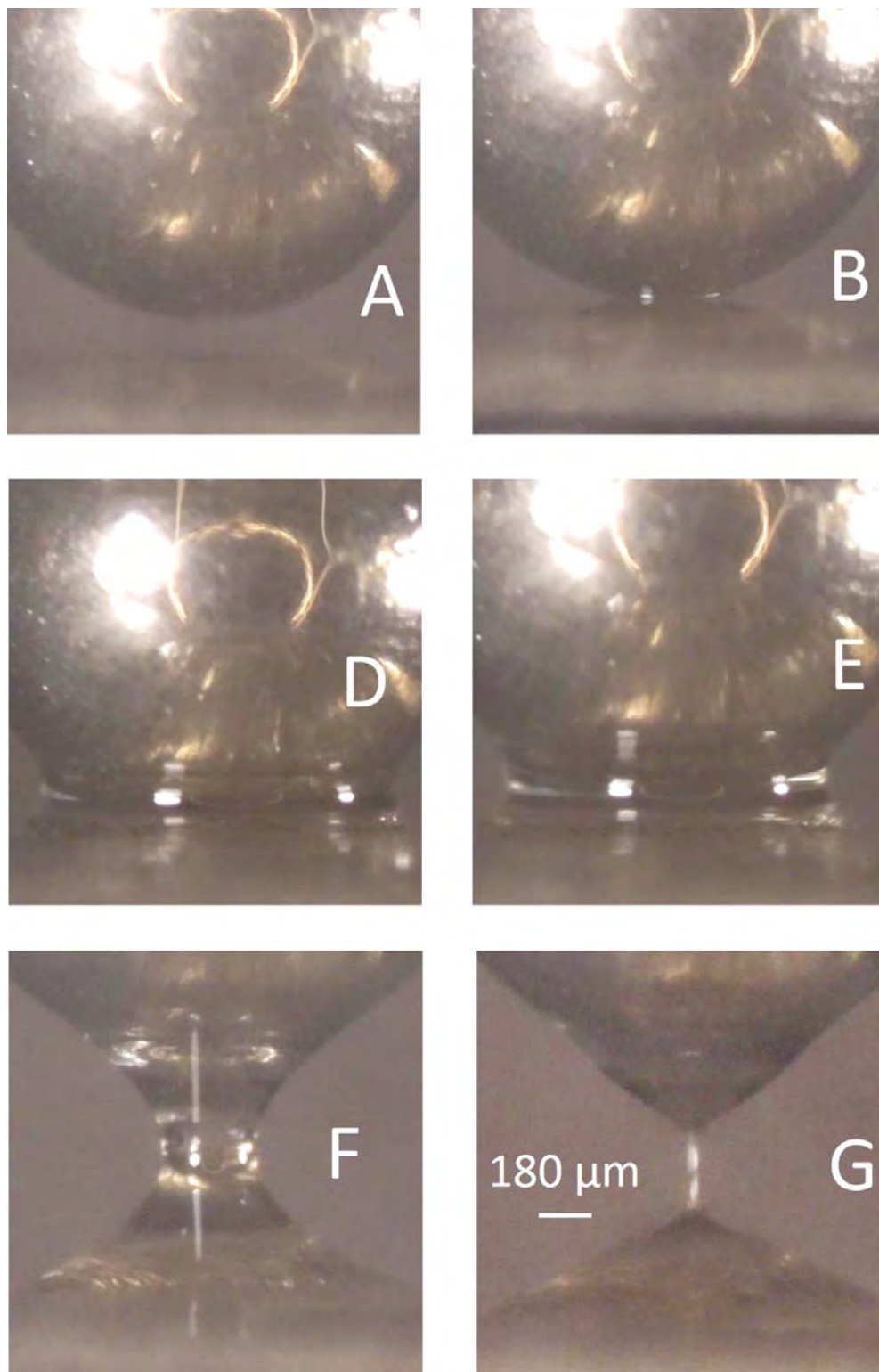


Figure 35: Pictures of the liquid bridge formed by silicone with marked regimes

4.2.2.2. EXPERIMENT WITH DI WATER

The viscosity of water is very less, so experiments with DI water is done to measure capillary forces without viscous effect. Stretching force in DI water is measured with respect to the length of the liquid bridge with the help of developed experimental setup. Raw data of the force vs displacement curve is shown in Figure 36. This raw data is filtered with 100 points moving average. The snapshot of the breaking of the liquid bridge portion with raw and filtered data is shown in figure Figure 37. This experiment is repeated with different speeds and results are shown in Figure 38 and Figure 39. The resultant curves of these experiments are superimposed as shown in Figure 40. This comparison shows that the nature of profiles for each experiment is the same as other experiment results for the same liquid. This comparison also indicates, jump in contact point moves forward with each repeated experiment. This can be due to evaporation of DI water from the surface of the cantilever. Further, this less quantity also may be responsible for changing the magnitude of the maximum attractive force. The maximum attractive force increases with decreasing quantity of DI water. Force vs time for DI water is plotted in Figure 41. This curve helps to recognise the effect of delay time between forwarding and backward motion. Here, the effect of draining of liquid towards the ball, while the actuator is not moving during delay time, changes the reaction force. This slow decay of force without stretching of the liquid bridge with respect to time can be utilised for calculation of viscosity of DI water.

Various regimes of stretching of DI water is represented in force vs displacement curve and force vs time curve as shown in Figure 39 and Figure 41 respectively. Explanation of regimes is given at paragraph 4.2.2. Pictures of these regimes for DI water is shown in Figure 42. Here regime 'A' shows approaching the ball towards DI water drop held at cantilever tip. At regime 'B' jump in contact happens and attractive force in DI water liquid bridge reached up to $-120 \mu\text{m}$. Regime 'C' shows further penetration of ball in DI water drop. At regime 'D', the positive force reached up to $80 \mu\text{N}$. At regime 'E', the formation of DI water liquid bridge, where attractive force increases as stretching increases. After achieving a maximum attractive force of $-200 \mu\text{N}$, regime 'F' starts. In this regime attractive force does not decrease sharply as compared to the silicone elastomer. The neck portion of DI water liquid bridge takes concave shape at this regime. The force is decay as a parabolic shape in this regime. Finally, the liquid bridge breaks suddenly due to the very low viscosity of DI water at regime 'G'. By observing Figure 40, it is also visible, the gap in maximum

attractive forces during forwarding motion and backward motion increases as the quantity of DI water decreases.

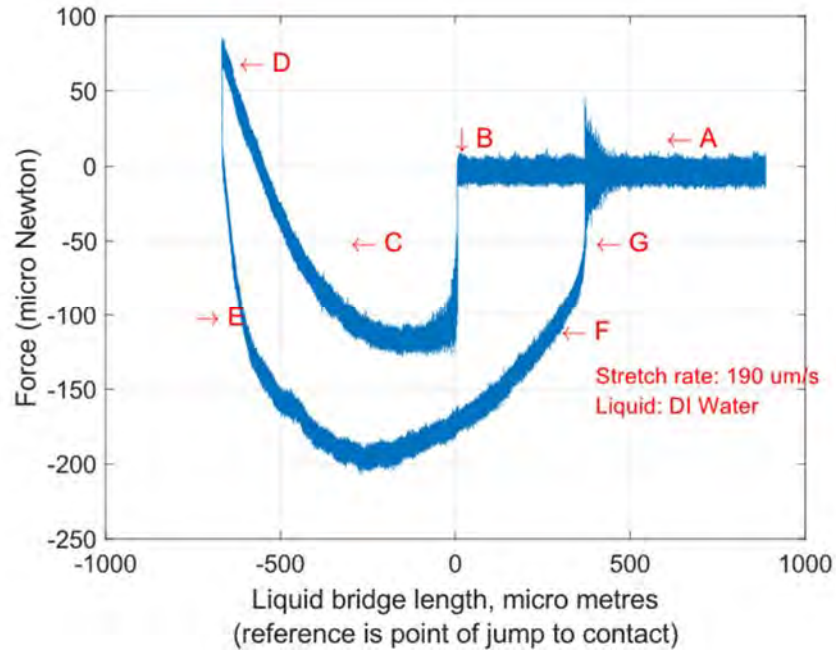


Figure 36: Force vs displacement curve with Raw data for DI water with a stretch rate of 190 $\mu\text{m/s}$

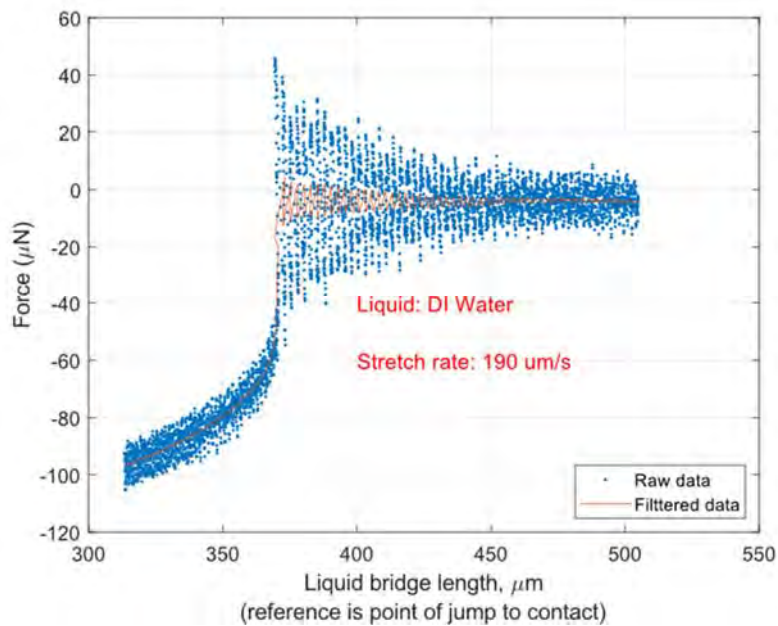


Figure 37: Raw data is filtered with 100 points moving average (snapshot of data at breakup) for DI water

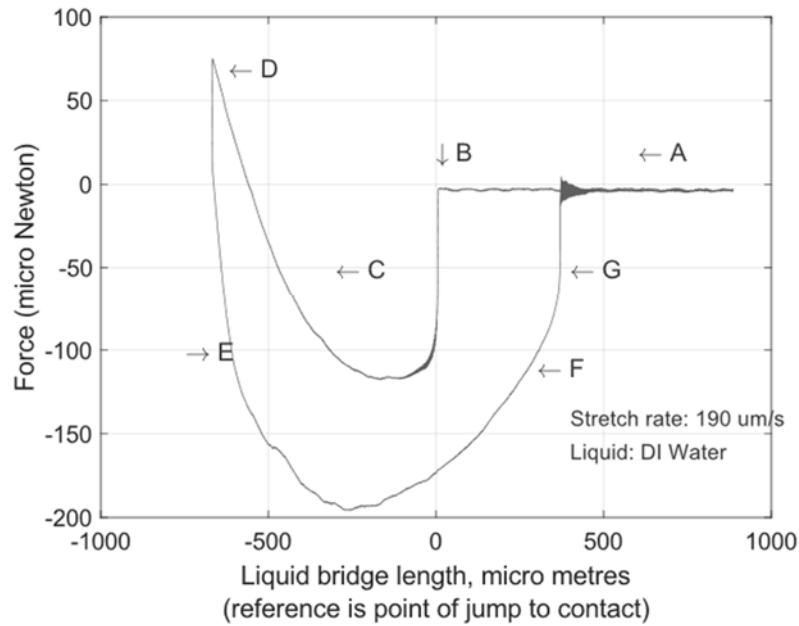


Figure 38: Filtered force vs displacement curve for DI water with a stretch rate of 190 $\mu\text{m/s}$

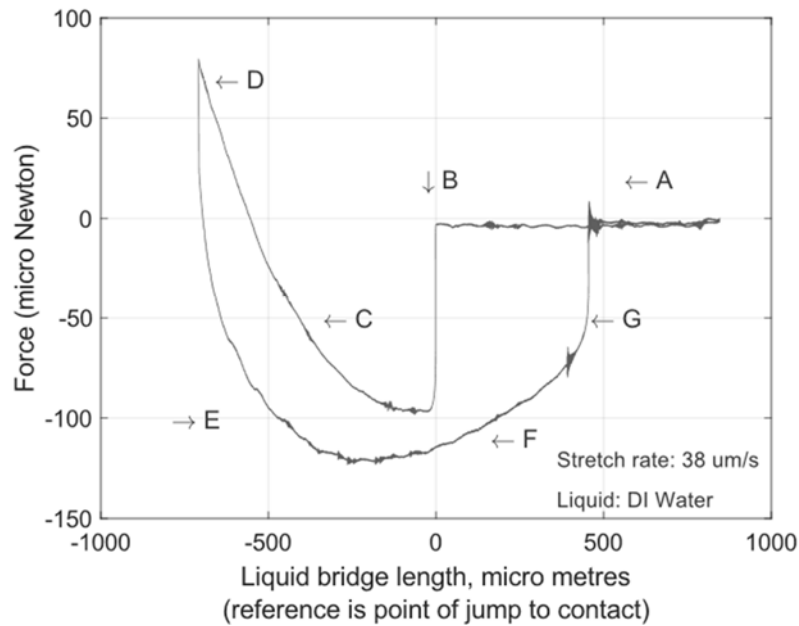


Figure 39: Filtered force vs displacement curve for DI water with a stretch rate of 38 $\mu\text{m/s}$

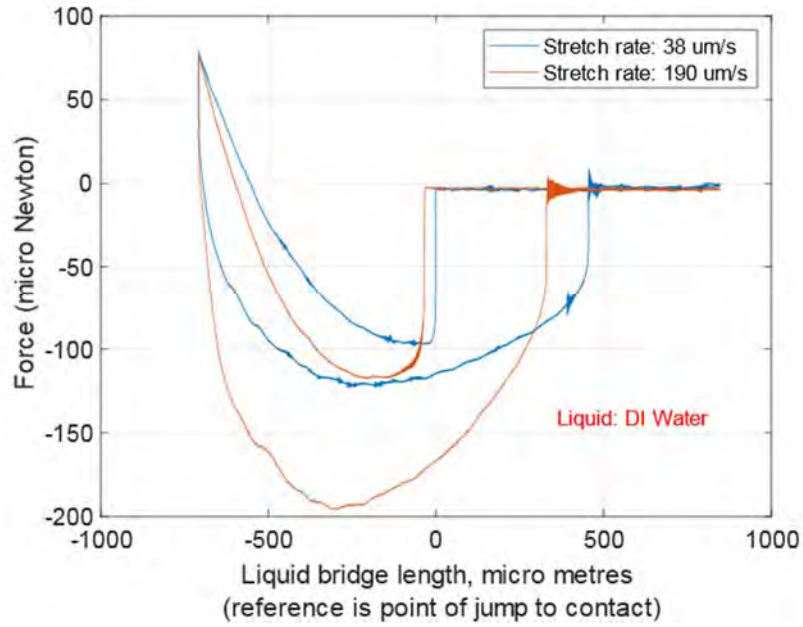


Figure 40: Compare with Filtered force vs displacement curve for DI water with different stretch rates

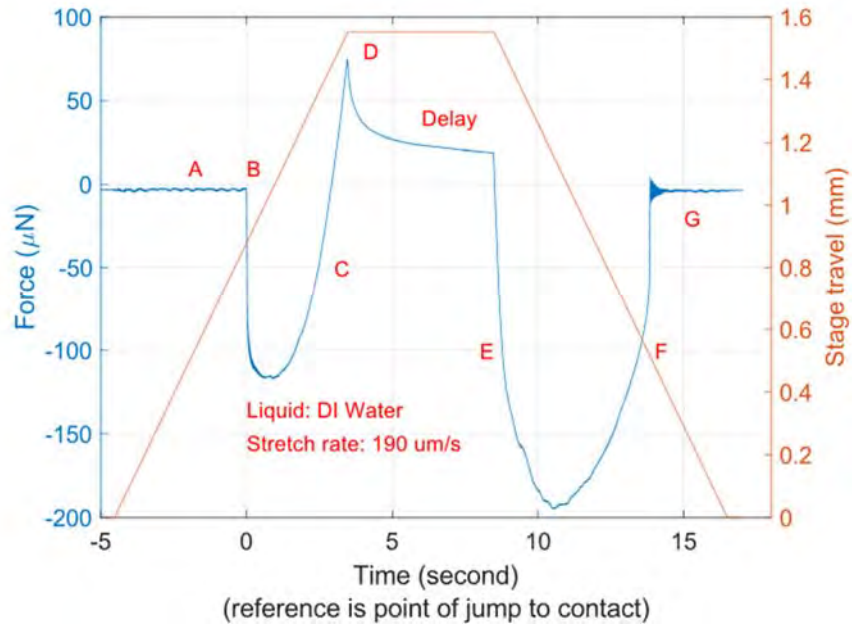


Figure 41: Filtered force vs time curve for DI water with a stretch rate of 190 $\mu\text{m/s}$

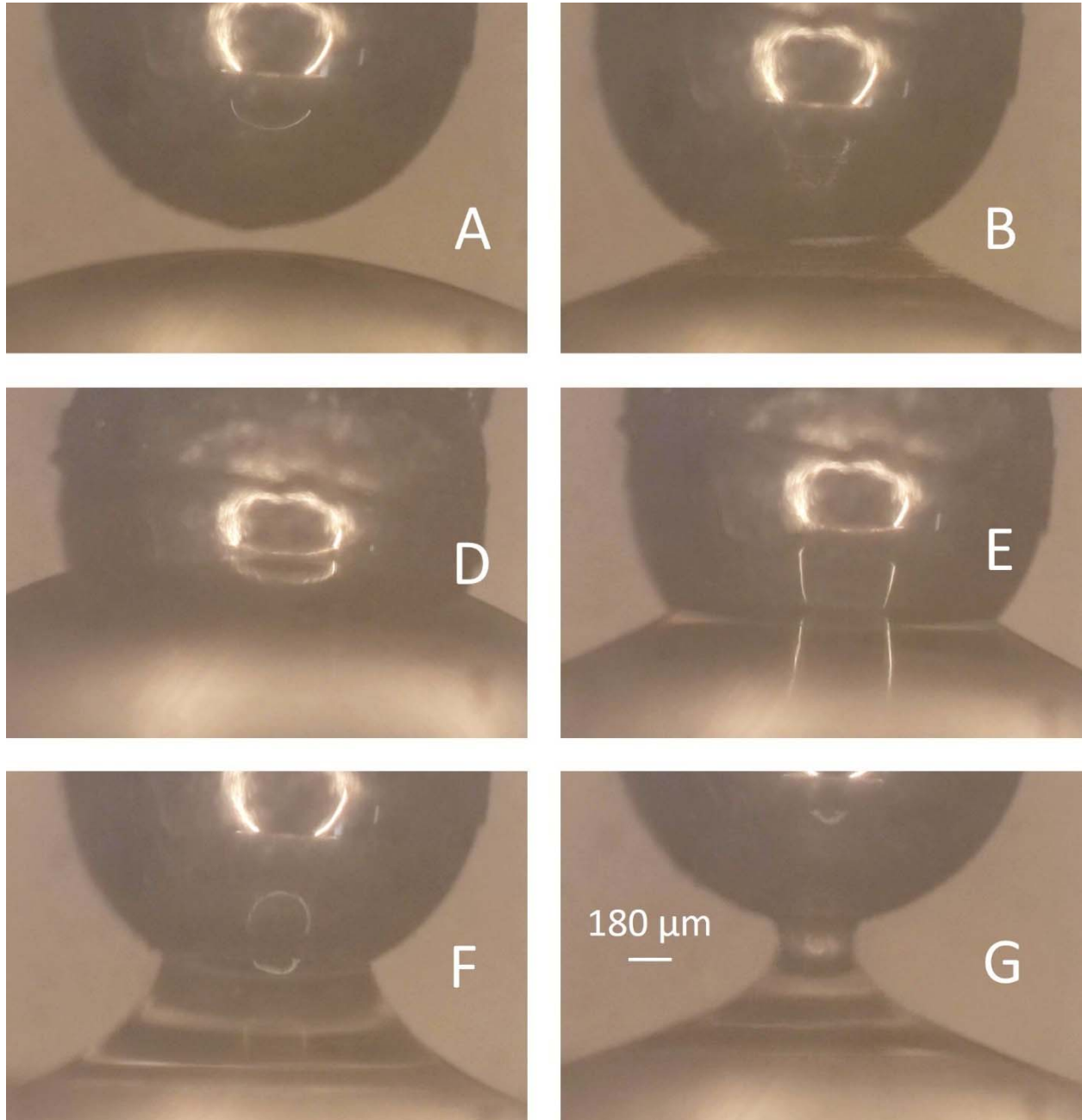


Figure 42: Pictures of the liquid bridge formed by DI water with marked regimes

4.2.2.3. EXPERIMENT WITH 1-DODECANETHIOL

Vapour pressure of Dodecane is very less as compared to water. Evaporation of DI water reduces the quantity of water which leads to changes in forces during experiments. To reduce evaporation effect, experiments with 1-Dodecanethiol is done. This replacement of liquid is done for improving repeatability in the experimental setup.

Stretching force in 1-Dodecanethiol is measured with respect to the length of the liquid bridge with the help of developed experimental setup. Raw data of the force vs displacement curve is shown in Figure 43. This raw data is filtered with 100 points moving average. The snapshot of the breaking of the liquid bridge portion with raw and filtered data is shown in figure Figure 44. This experiment is repeated with different speeds and results are shown in Figure 45, Figure 46 and Figure 47. The resultant curves of these experiments are superimposed as shown in Figure 48. This comparison shows that the nature of profiles for each experiment is remaining perfectly the same with other experiments with the same liquid. This comparison also indicates, jump in contact point does not move forward with each repeated experiment. This is due to very less evaporation of 1-Dodecanethiol from the surface of the cantilever. The further magnitude of maximum attractive force also remains the same for the experiment with 1-Dodecanethiol. Force vs time for 1-Dodecanethiol is plotted in Figure 49 and Figure 50 for two stretch rates. This curve helps to recognise the effect of delay time between forwarding and backward motion. Here, the effect of draining of liquid towards the ball, while the actuator is not moving during delay time, does not changes the reaction force. The ball completely immersed in liquid during forwarding motion, so this may be the reason for not changing forces during the delay time.

Various regimes of stretching of 1-Dodecanethiol are represented in force vs displacement and force vs time curves as shown in Figure 43 and Figure 49 respectively. Explanation of regimes is given at paragraph 4.2.2. Pictures of these regimes for 1-Dodecanethiol is shown in Figure 51. Here regime 'A' shows approaching the ball towards 1-Dodecanethiol drop held at cantilever tip. At regime 'B' jump in contact happens and attractive force in 1-Dodecanethiol liquid bridge reached up to $-160 \mu\text{m}$. Regime 'C' shows further penetration of ball in 1-Dodecanethiol drop. At regime 'D', the positive force reached up to $100 \mu\text{N}$. At regime 'E', the formation of the 1-Dodecanethiol liquid bridge, where attractive force increases as stretching start suddenly and further force decreases as stretching increases. This behaviour is different than DI water experiments. After this regime 'F' starts which is like regime 'E'. The reason for this effect may be due to the full immersion of ball during penetration. In this regime attractive force does not decrease sharply as compared to silicone elastomer. The neck portion of the silicone liquid bridge takes concave shape at this regime. The force is decay as a parabolic shape in this regime.

Finally, the liquid bridge breaks suddenly due to the very low viscosity of 1-Dodecanethiol. This regime is marked as ‘G’. By observing Figure 40, it is also visible, the gap in maximum attractive forces during forwarding motion and backward motion does not change with repeatable experiment. This effect is due to very less evaporation of liquid.

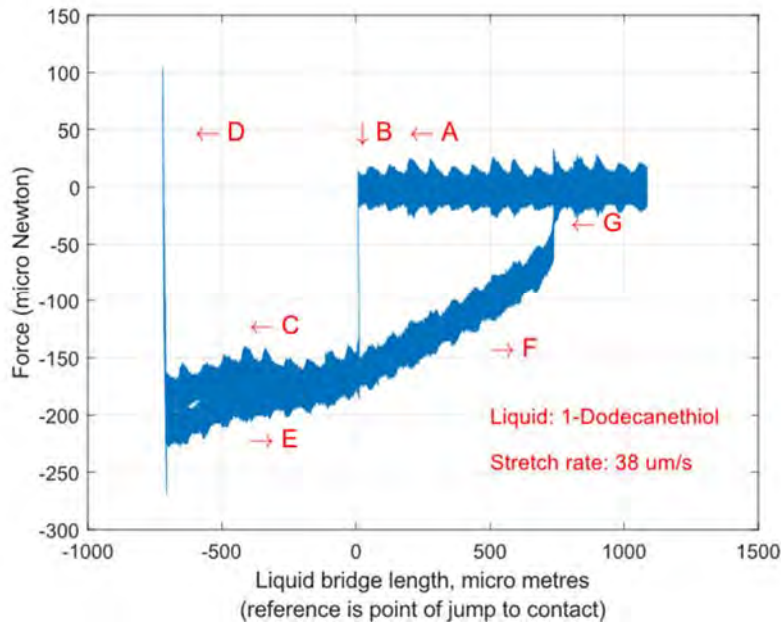


Figure 43: Force vs displacement curve with Raw data for 1-Dodecanethiol with the stretch rate of 38 $\mu\text{m/s}$

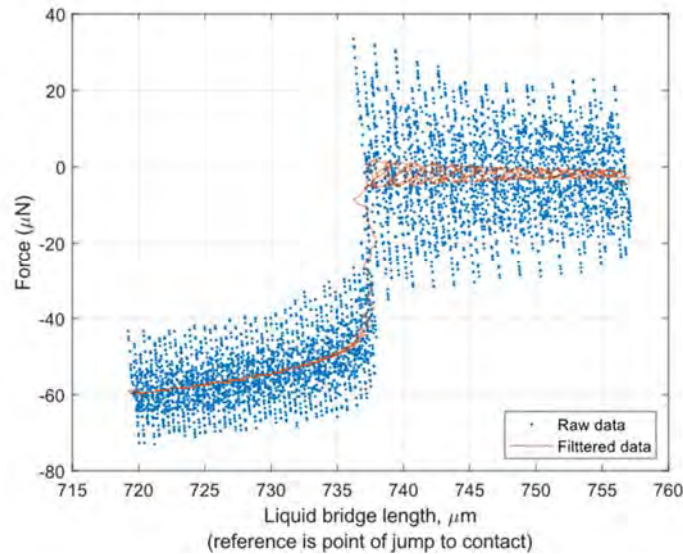


Figure 44: Raw data is filtered with 100 points moving average (snapshot of data at breakup) for 1-dodecanethiol

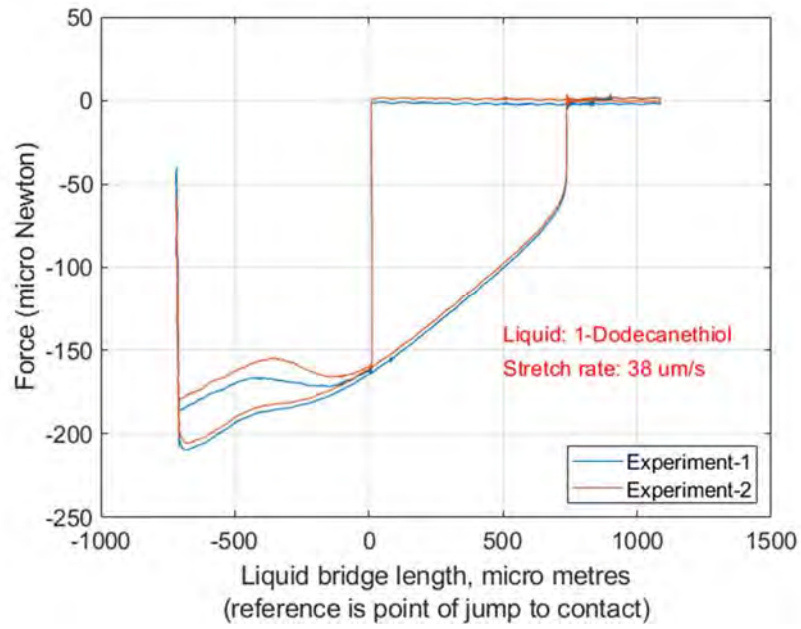


Figure 45: Filtered force vs displacement curve for 1-dodecanethiol with stretch rate $38 \mu\text{m/s}$

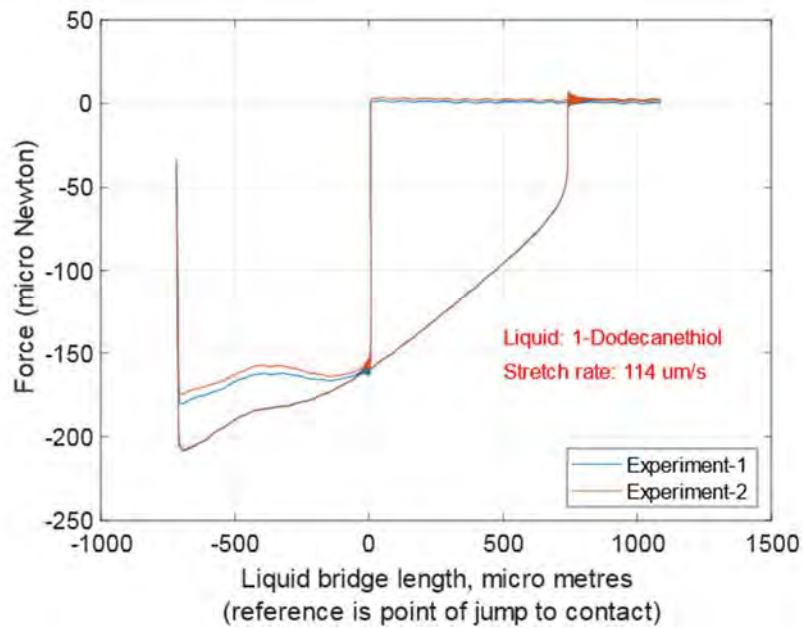


Figure 46: Filtered force vs displacement curve for 1-dodecanethiol with stretch rate $114 \mu\text{m/s}$

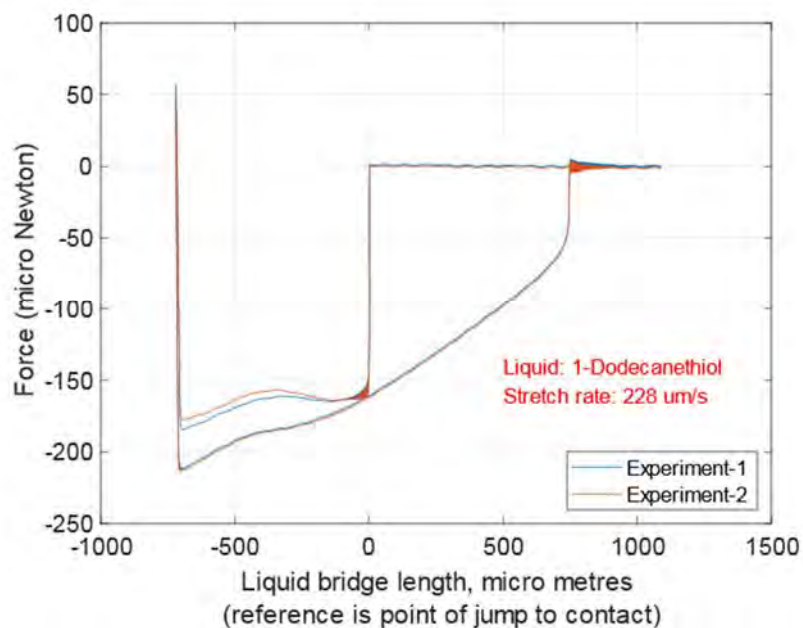


Figure 47: Filtered force vs displacement curve for 1-dodecanethiol with stretch rate 228 $\mu\text{m/s}$

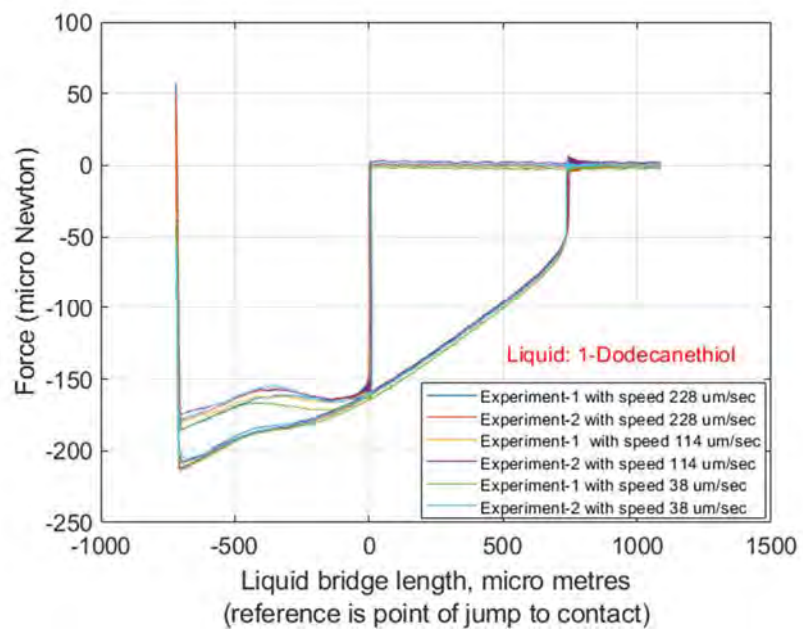


Figure 48: Compare with force vs displacement curve for 1-Dodecanethiol with different stretch rate

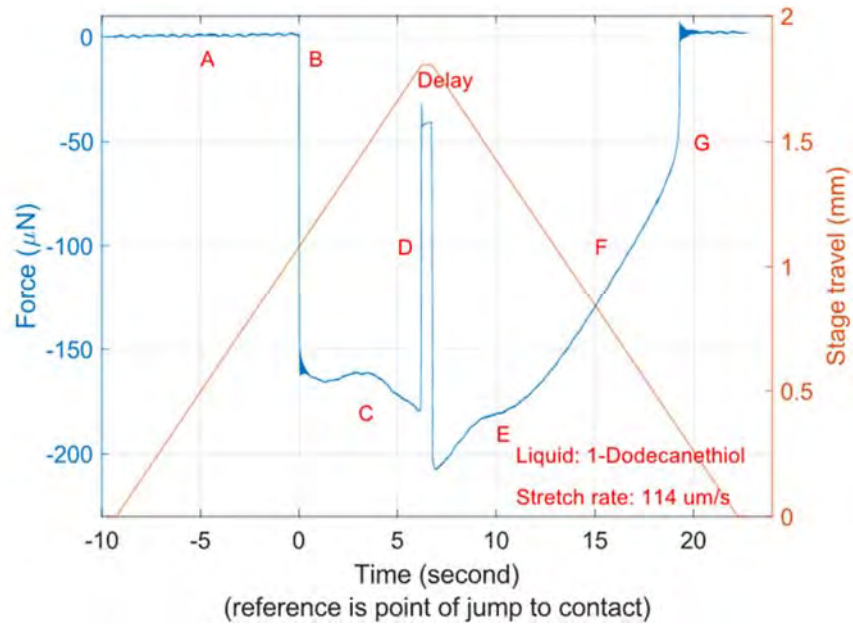


Figure 49: Filtered force vs time curve for 1-Dodecanethiol with stretch rate 114 $\mu\text{m/s}$

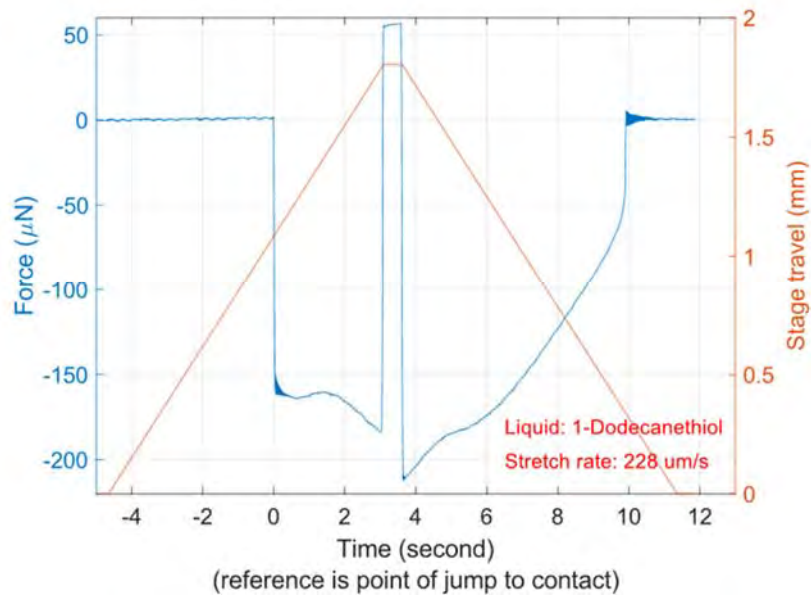


Figure 50: Filtered force vs time curve for 1-Dodecanethiol with stretch rate 228 $\mu\text{m/s}$

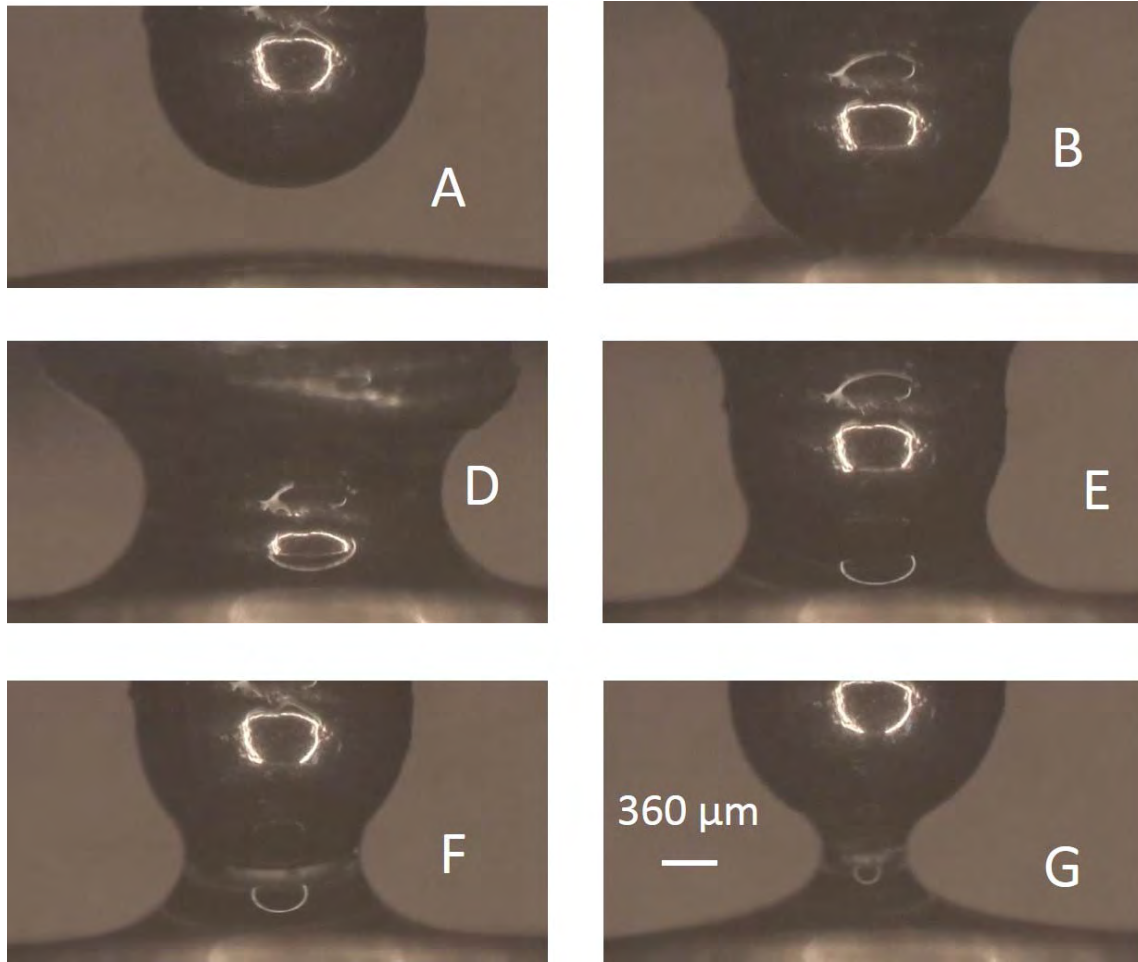


Figure 51: Pictures of the liquid bridge formed by 1-Dodecanethiol with marked regimes

4.2.2.3.1. FORCE CALCULATION FOR 1-DODECANETHIOL

Experimental results need to be verified with analytical results. Capillary force due to surface tension and Laplace pressure is calculated as per relations given at paragraph 2.5.2. The filling angle, the contact angle and the distance (Z_p) are measured from the snaps which were taken during experiments at time (T_f). The measured total capillary force at time (T_f) for 1-Dodecanethiol is almost near to experimental results. Two measurements with analytical results are shown in following table.

Table 2 Measurements and analytical results

PARAMETER	METHOD	VALUE FOR EXP-1	VALUE FOR EXP-2
Time (T_f).	recorded	8.1 Sec	9 Sec
Filling angle	Measured	50 degree	53 degree
Contact angle	Measured	5 degree	5 degree
Distance, Z_p	Measured	2.8 mm	3.1 mm
Capillary force due to surface tension	Calculated	-78 μN	-130 μN
Capillary force due to Laplace pressure	Calculated	-132 μN	-129 μN
Total Capillary force	Calculated	-210 μN	-260 μN

4.3. VISCOSITY MEASUREMENT

The liquid bridge is formed by a drop of silicone elastomer. This elastomer is a product of M/s Dow Corning, product code is Sylgard 184[28]. This liquid bridge is stretched by using the experimental setup as given at paragraph 4.2.1. This liquid bridge, as shown in Figure 52, is kept with a stretch condition where the neck region of the liquid bridge is formed. The liquid bridge length is stretched between 0.5 to 1.5 mm. As time passes, the neck part of the liquid bridge takes the cylindrical shape by its own. The picture of that instant is shown in Figure 53. The mid diameter of this cylinder is measured by comparing pixels of the diameter of the SS ball and diameter of the cylinder portion. The diameter of the SS ball is 1.8 mm. The neck radius ($R_{\text{mid}}(t)$) of the liquid bridge is measured 63.3 μm for one experiment. After a certain time, this neck of liquid bridge depleted automatically and finally, it breaks. Entire depletion and breaking of the filament of the liquid bridge are recorded by high definition, high frame recording camera, Sony RX100 V [26]. The setting for the frames captured is set 250 frames per second (fps) for this experiment. So, each frame is taken after 4 milliseconds. Entire recorded film of liquid bridge depletion is segmented in frames. By visual inspection of these frames, 'frame of cylindrical shape and frame of the breaking of filament' are selected. The difference is in both frames numbers is 41 frames for this particular experiment. So, the time required for braking is 0.164 seconds. Few intermediate frames of

filament breaking is shown in Figure 54 for this experiment. The viscosity is calculated as per theory has given at para 2.6.2. Surface tension (σ) of silicone elastomer is 20.9 mN/m as reported in [8]. The calculated viscosity of silicone elastomer is 9.09 Pa.s. As per the literature[8], the viscosity is measured 10.5 Pa.s for silicone oil (PDMS). This error can be reduced by better photography with proper lighting. This improvement will enhance the accuracy of measurement of the radius of filament. Recognition of correct frame, when the filament is broken, will also improve.

$$\eta_s = \frac{\sigma}{6R_{mid}(t)}(t_c - t) \quad (23)$$

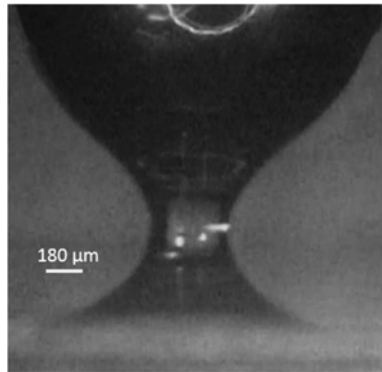


Figure 52: Liquid bridge after stretching and holding

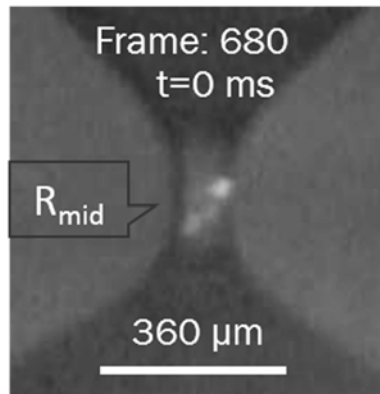


Figure 53: Neck of the liquid bridge, transforms in a cylindrical shape

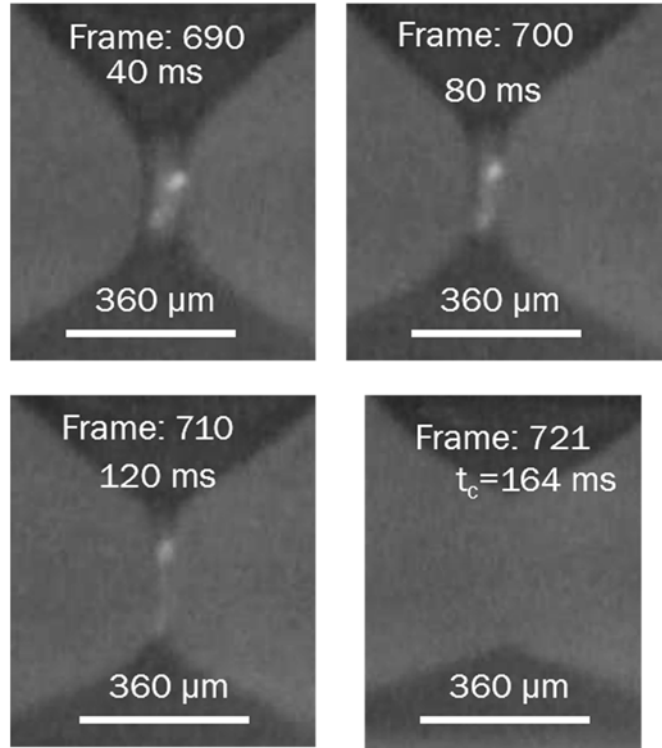


Figure 54: Intermediate frames of automatic depletion of the liquid bridge

Some more experiments were also carried out with different setting for measuring viscosity by stretching of liquid bridge. The experimental parameters and results are given below table

Table 3 Measurement of viscosity at different intervals

Experiment No	FPS, setting	R_{mid} (μm)	No of frames, to break the filament	(t_c-t) , ms	Viscosity (Pa.s)
1	1000	92	284	284	10.7
2	1000	71	194	194	9.4
3	1000	62	176	176	9.9
4	1000	80	293	293	12.8
5	250	28	24	96	12

4.4. DISCUSSION ON STRETCHING OF LIQUID BRIDGE EXPERIMENTS

By carrying out experiments with three different liquids, Silicone elastomer, DI water and 1-Dodecanethiol, few observations are surfaced out. Quasi-static and continuous stretching of the liquid bridge has different behaviour for viscous fluid e.g., silicone. But, slow and high stretching rate experiments, for negligible viscous fluids e.g., 1-dodecanethiol, have similar results. Liquids having less vapour pressure e.g., 1-dodecanethiol as compared to high vapour pressure e.g., DI water gives more repeatable results due to less evaporation of liquid from the sample. The viscosity of high viscous fluids e.g., silicone can be easily obtained by ‘the regime of breaking of filament’ as compared to low viscous fluids e.g., DI water and 1-dodecanethiol. Delay during forwarding motion and backward motion, where the liquid drains by itself on ball, has a significant role to increase the attractive force. This behaviour can be explored for calculation of viscosity of high and low viscous fluids simultaneously e.g., silicone and DI water. Attractive force in the liquid bridge, after achieving the maximum magnitude of attractive force during stretching of high viscous fluids e.g. silicone, decreases sharply and later it decays exponentially. But, attractive force in the liquid bridge, after achieving maximum attractive force during stretching of low viscous fluids e.g. DI water, decreases slowly and later it decays very fast. This effect is due to viscosity, viscous force dominates on capillary force and both are opposite nature during regime of breaking of filament. So viscous force does not allow the filament to break for viscous fluids and force decay very slowly.

CHAPTER 5

5. CONCLUSION AND FUTURE WORK

5.1. CONCLUSION

This work carried out to measure forces in the liquid bridge during extension of the liquid bridge for finding various regimes of stretching and calculating viscosity. An experimental setup is built during this project for measuring the attractive force developed in liquid bridge in range of $1\mu\text{N}$ to 3 mN . This range of force can be tailored by simple modification in the cantilever only. This experimental setup has capabilities of displacement control in resolution up to $0.38\ \mu\text{m}$ with up to 100 kilo samples per seconds recoding data in TDMS format for force measurement simultaneously. Provision for selection of stretch rate in wide range also provided in this setup from $3.8\ \mu\text{m/s}$ to $247\ \mu\text{m/s}$.

Various experiments were performed with different liquids with different stretching rates. Various regimes during formation and stretching of the liquid bridge in the experiment are marked in force vs displacement and force vs time curves for Silicone elastomer, DI water and 1-Dodecanethiol. The total magnitude of the capillary force and viscous force is measured during these experiments. Silicone elastomer shows highest attractive force during stretching of its liquid bridge, but repeatability does not establish due to drainage at the cantilever surface. Calculated and experimental force values for extension of DI water are found nearby but the evaporation of water leads to the change of values in each experiment. 1-Dodecanethiol shows clear repeatability with repeatable experiments with different stretching rates due to very lesser evaporation characteristics. The maximum attractive forces were measured $1.3\ \text{mN}$, $200\ \mu\text{N}$ and $210\ \mu\text{N}$ for silicone elastomer, DI water and 1-dodecanethiol respectably. Self-drainage of liquid, on ball towards the actuator side to achieve equilibrium during the delay between forward and backwards, was observed which changes the magnitude of attractive forces during halt condition.

The viscosity of silicone elastomer is measured in the range of 9 to 12 Pa.s during this work which is very closer to realistic values.

5.2. FUTURE SCOPE

There are some areas can be improved to increase accuracy in the experiment.

A stepper motor is used for a linear actuator which gives some small jerk in every step during slow speed. This jerk creates vibration in the system which further transmitted to the cantilever. So, the force data has noise at low magnitude. This problem can be rectified with a DC servo motor with a high precision optocoupler feedback mechanism.

A cantilever with the fiber optic displacement sensor is used for measuring force. The fiberoptic sensor is linear in a very narrow range. So, during full stretching of the liquid bridge, which can be more than 1 mm, the sensitivity of the displacement sensor can be changed. Frequent calibration of displacement sensor is also required due to change in reflectivity of the surface. So, to get, higher precision with accuracy in measuring forces, in the range of μN to mN , some different kind of sensor can be selected. Capacitive type sensor can be an option.

To measure dimensions of a liquid bridge, a digital camera is used. Triggering for the recording of the event with this camera i.e., start and stop is manual. So, the correlation between force data and the profile of the liquid bridge is manual. This can lead to introduce human error. A high definition, high frame rate recording, digital camera with integration with displacement control i.e. with LabVIEW, can be used to mitigating this human limit. Image analysis is done manually which can be done by some software (MATLAB) by comparing intensity graphs.

This work is carried out with three liquids. This experimental setup can be utilized to measure force-displacement and viscosity with a wide range of liquids, these liquids can have varied viscosity range from very low to very high. This will improve the understanding of physical phenomena on a small scale.

REFERENCE

- [1] P. V. Petkov and B. P. Radoev, “Statics and dynamics of capillary bridges,” *Colloids Surfaces A Physicochem. Eng. Asp.*, vol. 460, pp. 18–27, 2014.
- [2] T. Sridhar, V. Tirtaatmadja, D. A. Nguyen, and R. K. Gupta, “Measurement of extensional viscosity of polymer solutions,” *J. Nonnewton. Fluid Mech.*, 1991.
- [3] M. Binggeli and C. M. Mate, “Influence of capillary condensation of water on nanotribology studied by force microscopy,” *Appl. Phys. Lett.*, 1994.
- [4] Y. Men, X. Zhang, and W. Wang, “Capillary liquid bridges in atomic force microscopy: Formation, rupture, and hysteresis,” *J. Chem. Phys.*, vol. 131, no. 18, p. 184702, Nov. 2009.
- [5] A. M. Alencar, A. Majumdar, Z. Hantos, S. V. Buldyrev, H. Eugene Stanley, and B. Suki, “Crackles and instabilities during lung inflation,” in *Physica A: Statistical Mechanics and its Applications*, 2005.
- [6] B. N. J. Persson, “Wet adhesion with application to tree frog adhesive toe pads and tires,” *J. Phys. Condens. Matter*, 2007.
- [7] S. Cai and B. Bhushan, “Meniscus and viscous forces during separation of hydrophilic and hydrophobic surfaces with liquid-mediated contacts,” *Mater. Sci. Eng. R Reports*, vol. 61, no. 1–6, pp. 78–106, May 2008.
- [8] G. H. McKinley and A. Tripathi, “How to extract the Newtonian viscosity from capillary breakup measurements in a filament rheometer,” *J. Rheol. (N. Y. N. Y.)*, 2000.
- [9] P. A. Kralchevsky and K. Nagayama, *Particles at fluids interfaces and membranes : attachment of colloid particles and proteins to interfaces and formation of two-dimensional arrays*. Elsevier, 2001.
- [10] J. S. McFarlane and D. Tabor, “Adhesion of Solids and the Effect of Surface Films,” *Proc. R. Soc. A Math. Phys. Eng. Sci.*, 1950.

- [11] Y. I. Rabinovich, M. S. Esayanur, and B. M. Moudgil, "Capillary forces between two spheres with a fixed volume liquid bridge: Theory and experiment," *Langmuir*, 2005.
- [12] G. Lian, C. Thornton, and M. J. Adams, "A theoretical study of the liquid bridge forces between two rigid spherical bodies," *J. Colloid Interface Sci.*, 1993.
- [13] A. J. Lockwood, K. Anantheshwara, M. S. Bobji, and B. J. Inkson, "Friction-formed liquid droplets," *Nanotechnology*, 2011.
- [14] Z. Shi, Y. Zhang, M. Liu, D. A. H. Hanaor, and Y. Gan, "Dynamic contact angle hysteresis in liquid bridges," *Colloids Surfaces A Physicochem. Eng. Asp.*, 2018.
- [15] D. N. Mazzone, G. I. Tardos, and R. Pfeffer, "The behavior of liquid bridges between two relatively moving particles," *Powder Technol.*, 1987.
- [16] C. C. Liao and S. S. Hsiao, "Experimental analysis of dynamic properties in wet sheared granular matter," *Powder Technol.*, 2010.
- [17] J. Crassous, E. Charlaix, H. Gayvallet, and J. L. Loubet, "Experimental Study of a Nanometric Liquid Bridge with a Surface Force Apparatus," *Langmuir*, 1993.
- [18] O. Pitois, P. Moucheront, and X. Chateau, "Liquid bridge between two moving spheres: An experimental study of viscosity effects," *J. Colloid Interface Sci.*, 2000.
- [19] M. G. Bozkurt, D. Fratta, and W. J. Likos, "Capillary forces between equally sized moving glass beads: an experimental study," *Can. Geotech. J.*, 2017.
- [20] J. P. Cleveland, S. Manne, D. Bocek, and P. K. Hansma, "A nondestructive method for determining the spring constant of cantilevers for scanning force microscopy," *Rev. Sci. Instrum.*, 1993.
- [21] "Cambridge Polymer Group :: CaBER®." [Online]. Available: <http://www.campoly.com/cpg-services/electronics-and-hardware/instruments/caber/>. [Accessed: 05-Nov-2018].

- [22] P. Lambert, *Capillary Forces in Microassembly: modeling, simulation, experiments, and case study*. 2007.
- [23] L. M. Hocking, “The effect of slip on the motion of a sphere close to a wall and of two adjacent spheres,” *J. Eng. Math.*, 1973.
- [24] F. T. Trouton, “On the Coefficient of Viscous Traction and Its Relation to that of Viscosity,” *Proc. R. Soc. A Math. Phys. Eng. Sci.*, 1906.
- [25] “PHILTEC: Custom Fiberoptic Sensors for Non-Contact Measurement of Linear Distance, Displacement and Vibration.” [Online]. Available: <https://philtec.com/>. [Accessed: 06-Nov-2018].
- [26] “RX100 V The premium 1.0-type sensor compact camera with superior AF performance | DSC-RX100M5A | Sony IN.” [Online]. Available: <https://www.sony.co.in/electronics/cyber-shot-compact-cameras/dsc-rx100m5a>. [Accessed: 10-Jun-2019].
- [27] “USB 2.0 single-board camera with housing - mvBlueFOX-IGC - Industrial image processing.” [Online]. Available: <https://www.matrix-vision.com/USB2.0-single-board-camera-with-housing-mvbluefox-igc.html>. [Accessed: 14-Nov-2018].
- [28] T. Dow Chemical Company, “SYLGARD™ 184 Silicone Elastomer,” 2017. [Online]. Available: www.consumer.dow.com. [Accessed: 10-Jun-2019].
- [29] A. C. M. Kuo, “Poly(dimethylsiloxane).”